Electronic and Optical Properties of Two-dimensional Heterostructure and Homobilayer with various interlayer Twist angle

By

RAJESH BISWAS

Registration No. 154098 of 2020-2021

Exam Roll No. M4ETC22029

With the Guidance of

Dr. Divya Somvanshi

Thesis Submitted in partial fulfillment of the requirement for the award of the Degree of Master of Engineering in Electronics and Telecommunication Engineering

Department of Electronics & Telecommunication Engineering

Jadavpur University

kolkata-700032

June 2022

Faculty of Engineering & Technology

Jadavpur University

CERTIFICATE OF RECOMMENDATION

I hereby recommend that this thesis prepared by **Rajesh Biswas** entitled **"Electronic and Optical Properties of Two-dimensional Heterostructure and Homobilayer with various interlayer Twist angle"** with my supervision be accepted for partial fulfillment of the requirements for the award of the Degree of Master of Electronics and Telecommunication Engineering.

.....

Dr. Divya Somvanshi

Thesis Supervisor

Department of Electronics and Tele-Communication Engineering

Jadavpur University, Kolkata – 700032

.....

Prof. Ananda Shankar Chowdhury

Professor and Head of the Department

Department of Electronics and

Tele-Communication Engineering,

Jadavpur University, Kolkata – 700032

.....

Prof. Chandan Mazumdar

Dean

Faculty Council of Engineering and Technology

Jadavpur University, Kolkata – 700032

FACULTY OF ENGINEERING & TECHNOLOGY

JADAVPUR UNIVERSITY

DEPARTMENT OF ELECTRONICS &

TELECOMMUNICATION ENGINEERING

CERTIFICATE OF APPROVAL*

The foregoing thesis is hereby approved as a credible study of an Engineering subject carried out and presented in a manner satisfactory to warrant its acceptance as prerequisite to the Degree for which it has been submitted. It is withstand that by this approval, the withsigned don't necessarily endorse or approve any statement made, opinion expressed or conclusion drawn therein but approve the thesis only for the purpose for which it is submitted.

Committee on

Final examination for

Evaluation of the Thesis of

RAJESH BISWAS

Exam Roll No: M4ETC22029

.....

.....

Signature of Examiners

*Only in case the thesis is approved.

DECLARATION OF ORAGINALITY AND COMPLIANCE OF ACADEMIC ETHICS

I hereby declare that this Thesis contains literature survey and original work by the withsigned candidate, as part of his Master of Electronics and Telecommunication Engineering studies.

All information in this document have been obtained and presented in accordance with academic rules and ethical conduct.

It is also declare that, as required by these rules and conduct, I have fully cited and referenced all materials and results that are not original to this work.

Name of the Candidate : Rajesh Biswas

Examination Roll No. : M4ETC22029

Thesis Title : "Electronic and Optical Properties of Two-dimensional Heterostructure and Homobilayer with various interlayer Twist angle".

Signature of the Candidate :

Date:

ACKNOWLEDGEMENT

I express deep sense of gratitude and indebtedness to my Thesis Supervisor, Dr. Divya Somvanshi, DST INSPIRE Faculty of the Department of Electronics & Tele-Communication Engineering, Jadavpur University, Kolkata, for providing me the opportunity to carry out the Thesis work. I am grateful to her for the valuable insights and suggestions that he gave me throughout my M.E. report.

I am thankful to and fortunate enough to get such a nice support, devotion and constant encouragement from my senior, Ms. Sayantika Chowdhury throughout my thesis work. She supported me in guiding, inspired me to strive towards my goal.

I would also like to thank, Prof. Ananda Shankar Chowdhury, Head, Department of Electronics & Tele-Communication Engineering, Jadavpur University for his compassionate approach. I would like to express my sincere gratitude to all the teaching and non-teaching staffs of the department for providing necessary support.

Last but not the least, this work would not have been possible without the love, support and encouragement of my family, classmates and near and dear ones. I want to give special thanks to my friend Ms. Trisha Mallick, for supporting me throughout this journey.

RAJESH BISWAS

Abstract

Discovery of two-dimensional (2D) material have brought multiple ways to modify electronic structure and optical properties of materials and devices at atomistic level. There is verity of 2D materials available in research community. Among those 2D-Transition-metal dichalcogenides (TMDC) materials hold some very important and interesting properties. Therefore, in our thesis work we are mainly focussed on TMDC materials. At present, world is suffering from pollution where non-renewable energy sources are major cause. To overcome this issue, we should move to renewable energy sources such as hydrogen energy, solar energy etc. Here the 2D materials plays important role as they are much more efficient material than any other material. The Home/hetero structures and based on 2D materials also playing a very important role in various applications such as Photocatalyst, photodetectors, sensors wearable electronics etc.

The properties of 2D home/hetero structures varied by different factors such as mechanical strain, external electric field and twist angles. Therefore, in the work, we used twist angle as a external factors to modulate the properties of $MoSe_2/MoSe_2$ homo bilayers and $GaTe/MoS_2$ based heterostructures. One of our main focus throughout the this work is to find such selective angles so that properties are modified as per application requirement.

Contents

List of Figures

List of Tables

Abbreviations

2D	Two Dimensional
TMDC	Transition Metal Dichalcogenide
DFT	Density Functional Theory
PDOS	Projected Density of States
vdW	Van der Walls
vdWH	Van der Waals Heterostructure
BSSE	Basis Set Superposition Error
LCAO	Linear Combination of atomic Orbitals
CP	Counterpoise
$MoSe_2$	Molybdenum Diselenide
GaTe	Gallium Telluride
MoS_2	Molybdenum Disulfide
ELF	Electron Localization Function
GGA	Generalized Gradient Approximation
PBE	Perdew–Burk e–Ernzerhof
CBM	Conduction Band Minima
VBM	Valance Band Maxima
eV	Electron Volt

Chapter 1

Introduction

1.1 Introduction to 2D Material

The 2D materials are being attracted by community of the researcher around the globe due to its unique and excellent properties. Graphene was the first 2D material to be discovered in the year 2004 by mechanical exfoliation, which brings the revolution of 2D materials. After discovery of Graphene, several other 2D materials discovered, and a lot of research is going on. In the multilayer of 2D materials including Graphene the atomic layers are combined by van der waals (vdW) forces. Ongoing research on 2D materials has opened different domain of band gap engineering by applying mechanical strain, thickness variation, external electric field, interlayer twist, etc. Among all the available techniques the interlayer twist and application of external electric field have greatly encouraged by the researcher for analysing novel physical phenomena in this field. As an example: the inherent superconductivity is unusual [2] , insulating behaviour [3] reconstruction on an atomic scale,[4] and transportation via a topological channel network [4, 5] can be made by twisting two Graphene sheets together at a slight angle. It is found that in MoS_2 homo-bilayer there exist ultra-flat bands in the moire pattern which is caused by the structural reconstruction[6]. Band engineering has opened a band gap in the bilayer Graphene [7, 8] and also it has made possible to covert TMDC from semiconductor to metal and many other interesting observations [9] The TMDC material is being found to have many important effects such as piezoelectricity, layer locking effects on spin, oscillations of Shubnikov-de Haas type etc. This effects made this TMDC material as favourable 2D material for its superior performances [10] [11, 12]. In BP-WSe_2 based p-n

junction diode , it has a stated external quantum efficiency of 23 % with an open circuit voltage of 0.35 volt, and a power conversion efficiency of 1.7 percent.

Basically, 2D materials are the crystalline materials which have single or multi-layer atoms and in which there are in plane strong interatomic forces and weak vdW interlayer forces. That's why it is possible to exfoliate as many layer as it is required. 2D materials have long list of materials which includes many other categories of materials other than Graphene. Boron nitride, TMDCs, Mxenes are some of the example. The 2D family of materials offers every a wide range of materials ranging from metallic, semi-metallic, insulating, superconducting etc.[13]. The 2D atomic crystals are stable and this fact itself amazing. According to the theorem of Mermin-Wagner there should not be 2D long-range order. Thus, at any finite temperature dislocations should appear in 2D crystals [14]. The traditional theory has been predicted that lack of long range order in two dimensions is because of logarithmic divergencies. However, it is possible to make very high quality stable 2D crystal with finite size. Also this can be mass-produced in vast numbers and make them a qualified candidate for exciting applications. These class of 2D materials have brought immense research interest because of its thickness uniformity at the monolayer without any surface dangling bonds[15, 16].

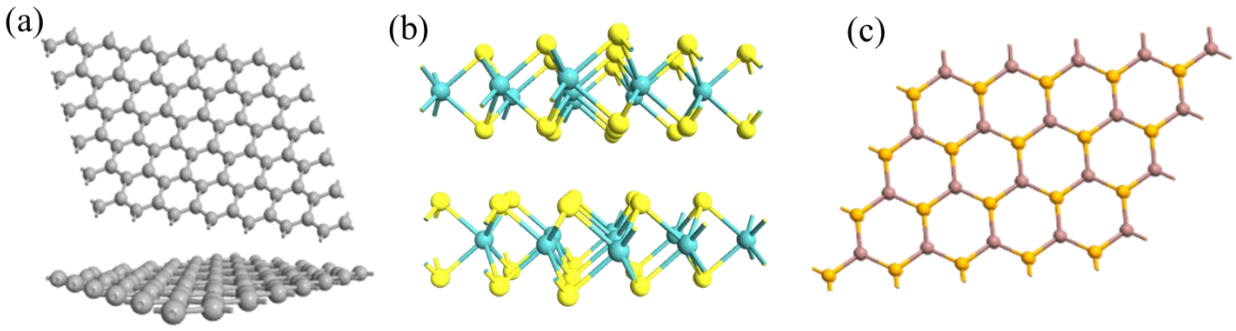

Figure 1.1 Schematic atomic structure of various 2D Materials (a) Graphene (b) MoS_2 (c) InSe, clearly shows hexagonal arrangement of atoms.

1.2 TMDC Materials

Atomically thin TMDCs are a semiconductor material in the family of 2D materials These materials have general formula of MX_2, where M represents a transition metal in the periodic

table (such as molybdenum, tungsten, etc.) and X represents chalcogen atom (such as sulphur, selenium, tellurium, etc.). In TMDC, the layer of M atoms are being sandwiched between two layer of X atoms. The layers are vertically attached by weak vdW force[17, 18]. The intralayer M-X bonds in TMDC are covalent bonds and it is significantly more powerful than vdW force. The different structural polytypes that a TMDC materials exists are of three different phases such as 1T, 2H and 3R where, The numbers in the c axis represent the number of X-M-X sandwiches per unit cell. While T, H, R representing the crystal symmetry of tetragonal, hexagonal and rhombohedral respectively. For example, MoS_2 exist in eight 2H or 1T phase, The 1T phase is a metastable metallic phase, while the 2H phase in the c axis is a thermodynamically stable state unit cell [19].

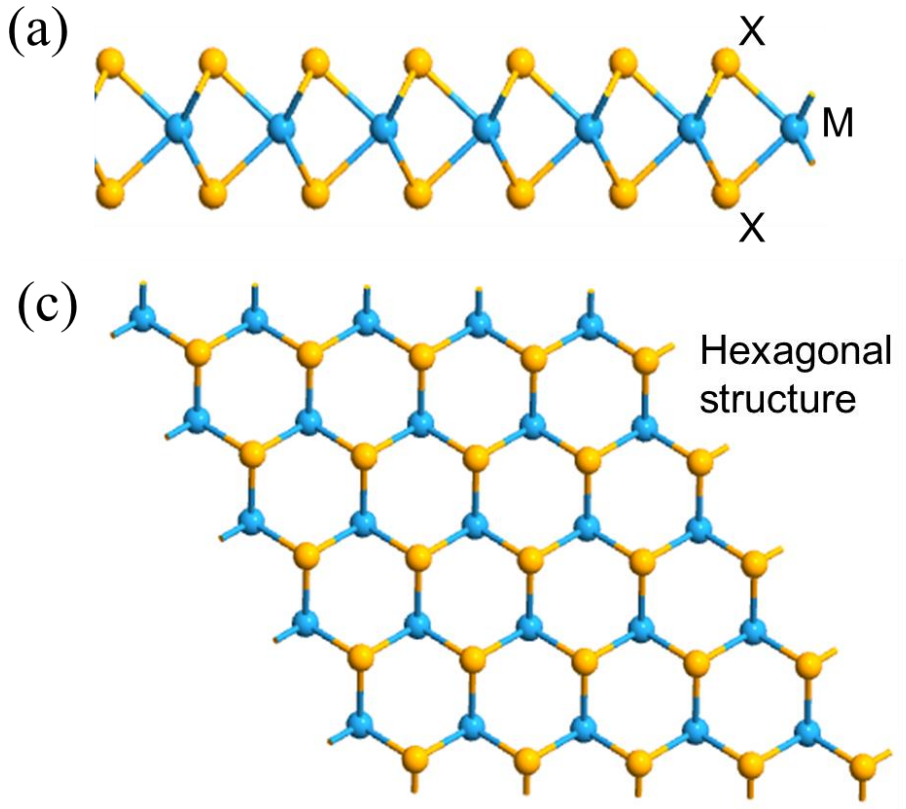

Figure 1.2 shows (a) monolayer TMDCs, where M is transition metal atom and X is chalcogenides materials (c) Hexagonal structure of monolayer TMDC materials

1.3 Density Functional Theory (DFT)

In quantum mechanics, the quantum mechanical wave function contains all of the information about a specific system. To derive the wave function of a system, we can solve the Schrodinger equation perfectly for a simple 2D material or even a hydrogen atom. The permissible energy states of the system can then be determined.

$H(r_1, r_2, \ldots, R_1, R_2, \ldots) = E(r_1, r_2, \ldots, R_1, R_2, \ldots)$,

Where $(r_1, r_2, \ldots, R_1, R_2, \ldots)$ is a wave function, which corresponds to the positions of electrons, r_i, and the nuclei R_I.

The Schrodinger equation for an N-body system is, unfortunately, impossible to solve. We can, however, approximate a solution to the Schrodinger equation of a many-body system using DFT [20, 21]. The features of an interacting many electrons system can be characterised by a functional of the electron density that is a function of space and time, which is the basis of DFT. In DFT, the electron density is a key fundamental feature [22]. The electron density is merely a function of x, y, and z, only three variables, while the electronic wave function for numerous bodies is a function of 3N variables (the coordinates of all N atoms in the system).

The DFT formalism arose from Hohenberg and Kohn's ground breaking work, which presented a theorem that indicates an exact theory of many body systems. The two most essential foundational theorems in DFT (Hohenberg–Kohn and Kohn–Sham) explicitly state the relationship between total energy and electron density.

Theorem-1: "The ground state of all interacting many particle systems with a given fixed inter particle interaction is a unique functional of the electron density n(r)," according to the first Hohenberg–Kohn theorem, published in 1964[23]. It states that a system's density determines all of the system's ground-state attributes. The overall ground state energy of a many-electron system is a function of density in this case.

i. e. $E = E[n(r)]$.

Theorm-2 When the non-interacting kinetic energy functional Ts is included into the energy expression, it results in a set of one-particle equations whose solutions are the Kohn–Sham orbitals after functional differentiation[24]. "The real ground state electron density is the

electron density that minimises the energy of the overall functional," it says i.e., E [n(r)] > $E_0[n_0(r)]$

However there are some limitations in DFT, (1) even for very small N number system it is highly trivial and causes wave functions a complicated objects, (2) the computational time goes very rapidly if N becomes very large.(The number of atoms in the system is denoted by N) To solve this there is an alternative approach that has been taken. Instead of using a many-body wave function as a fundamental theorem, a single body or one body system is used. Because rather than the 3N coordinates of the wave function, density n(r) is a function of only three spatial variable, it can be computed even for enormous systems[25].

1.4 Twistronics

1.4.1 Introduction to Twistronics and Moire Lattice

Twistronics is the field of material science where interlayer relative rotational angle or the twist angle is used as a control variable for tune the electronic and optical properties of two-dimensional materials. It can dramatically change the material properties after applying interlayer twist and this effect is very unique[26]. It is being first applied to the bilayer Graphene system. For Graphene a very small twist angle less than 1.1° can alter its flat band condition to introduce band gap in bilayer Graphene.

New periodicities develop when two periodic functions – even two simple cosine functions – are effectively multiplied. So if two lattices or crystals are efficiently multiplied, a new periodic lattice known as moiré pattern will be emerged. Comprehending the concept of a moiré pattern – and the building of a moiré superlattice – is the first step in withstanding the origin of twist-dependent characteristics. Moiré refers to two layers of damp silk pushed together and it has a French derivation. An interference pattern is generated as the layers slide across one another. Moiré patterns are generated when two lattices slide across one other [27]. Twistronics, which emerges from the moiré superlattice of the narrow angle between twisted bilayers of two-dimensional materials like Graphene, has sparked a lot of curiosity in the domains of 2D materials and condensed matter physics. When the twist reaches specific magical angles, a dispersion less flat band forms, resulting in unexpected physical properties such as

unconventional superconductivity. The required effects can be accomplished by modifying the filling of the fourfold degeneracy flat bands due to the close coupling of the degenerated Bloch electrons [28]. Moire superlattices are formed by the periodic overlapping of orbitals and the rebuilding of lattices between high atomic registry positions in two-dimensional layered materials that are vertically stacked. These are quantum activated interfaces in which non-trivial quantum phases can originate from the geometric placements of two-dimensional materials, and the two-dimensional materials are not intrinsic to the parent materials in this case. Long-range correlations, charge-ordering, and a variety of other exciting quantum effects are hidden inside the physical location among the (same type or different) parent materials due to unanticipated aberrations in band structure and topologies. These superlattices, which might be layered, twisted, gate-modulated, and optically stimulated, provide a new window into physics in a many body and topological framework from the weak to strong correlations limit.[27].

The moiré pattern, which can be thought in the form of a unit cell with unique vectors, generates a new long-range periodicity. The new superlattice (or supercell) that is generated is then identified and specified using these vectors. Where m, n, r, and s must all be integers, a and b and c are the lattice vectors for each parent material, Eq. 1 is the Diophantine equation that must be met to form a commensurate unit cell. The moiré superlattice formed is reliant on both the ratio of lattice constants and the twist angle since the lattice vectors contain information about the lattice constant and its orientation in space. Additional information on mathematically producing moiré patterns for 2D materials applications in theory and practise, including grain boundary identification, may be found in the following references[29-35].

$$v_{moiré} = m \times \vec{b}_1 + n \times \vec{b}_2 = r \times c_1 + s \times c_1 \quad (1)$$

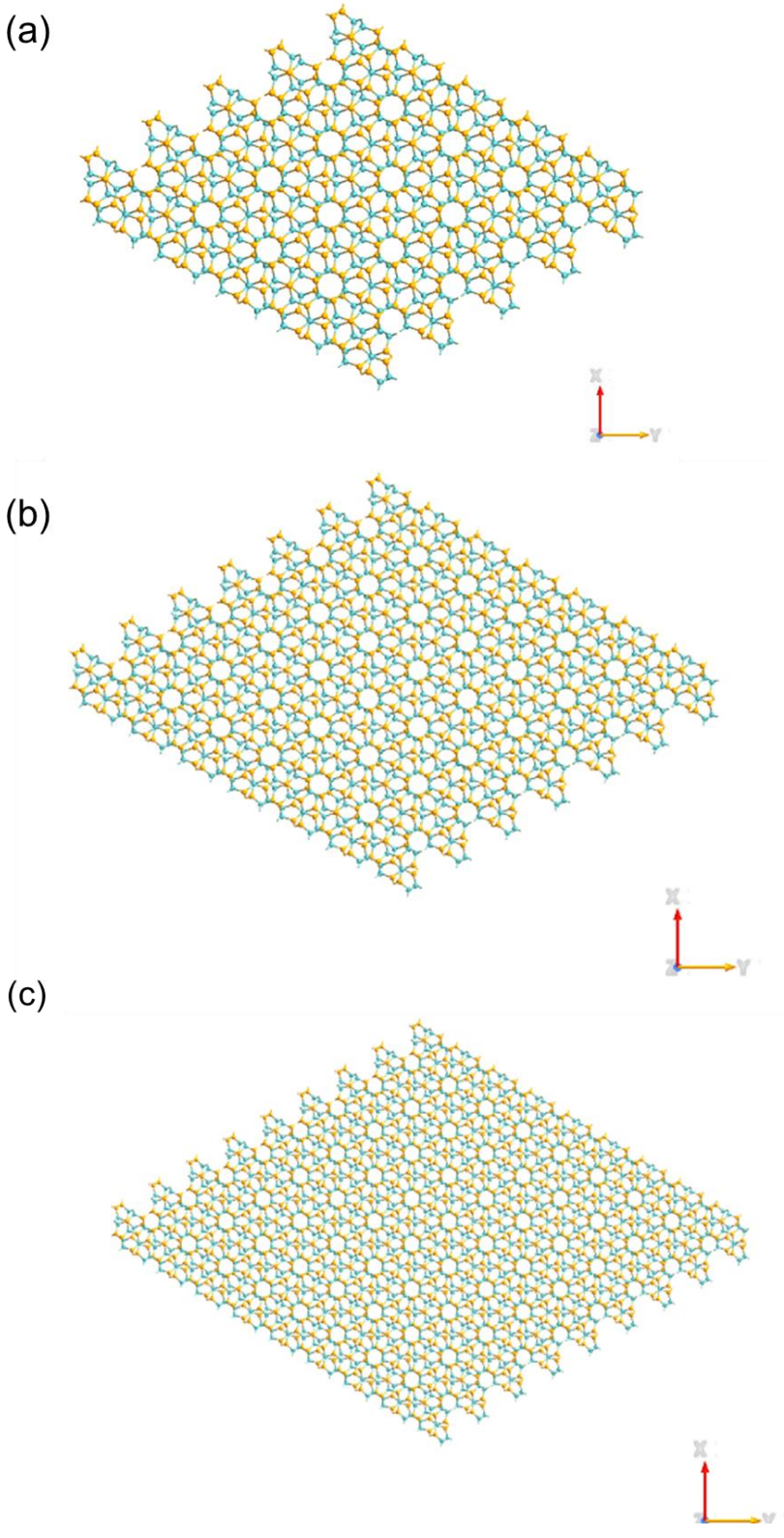

Figure 1.3 Schematic atomic structure of twisted structure with varying super cell size (a) 5×5×1 (b) 7×7×1, (c) 11×11×1

1.4.2 Magic Angles

The impact is so transforming in particular 2D structures that the matching twist angles are referred to as "magic.". As of Ref [3, 36-38], Superconductivity, orbital ferromagnetism, moiré excitons, the quantum anomalous Hall effect, strong electron correlations, both intra and interlayer exciton photoluminescence, twist dependent colour, Hofstadter Butterfly, Topological channels in one dimension, quantum fractal hall effect, lateral as well as vertical conductivities, and vertical conductivities that are spatially dependent have all been shown to manifest from the magic twist angle phenomenon. According to a substantial body of research, the twist angle appears to be just as crucial as other important factors such as doping, stoichiometry and crystal structure, a have enormous potential for technologies of the future generation. In reality, even modest changes with twist angle can have a significant impact [3, 4, 38, 39] . This naturally raises the question of how and why the twist angle affects the band structure and properties of 2D materials so dramatically. In a nutshell, the solution is because of the moiré pattern formed by the interaction between the layers, which results in the formation of a new periodic super lattice with a distinct band structure. With this in mind, atomic reconstruction (the movement of atoms due to a mixture of inter- and intra-layer bonding) has a substantial impact on the moiré pattern (and moiré superlattice). Interlayer bonding produces a force that induces atom repositioning, depending on the particular 2D structure and twist angle, with the equilibrium configuration being a balance between the interlayer and intra-layer bonding. This effect appears only when the interlayer coupling is strong enough to allow for effective interlayer bonding. Furthermore, as the twist angle changes, the moiré pattern changes, hinting that the superlattice – and its associated band structure – changes as well.

1.4.3. Mathematical Modelling

There are few things to consider before diving into mathematical modelling.

(1) Monolayer TMDCsmimic Graphene in both direct and reciprocal lattice vector spaces.

(2) Layer 1 has two sublattices, A and B, whereas layer 2 has two sublattices, A_0 and B_0. In an AB stacked bilayer, the horizontal positions of A and B_0 atoms are identical.

(3) A comparable structure is generated when a B_0 atom is rotated to a position previously occupied by an atom of the same kind.

In condensed matter physics, Graphene, a 2D carbon crystal, is the only substance capable of realising the massless Dirac equation. The symmetry of the Graphene honeycomb lattice causes a linear energy-momentum dispersion and an internal degree of freedom equal to chirality for low energy excitations, features that are similar to massless Dirac fermions. This leads to a slew of unexpected electronic features, such as an anomalous phase in the integer quantum Hall effect, B-dependent Landau level energies, and suppressed backscattering, which leads to quasi ballistic transport [40].

Few-layer Graphene(FLG systems, which consist of two or more atomic layers of Graphene, also produce rich and novel physics. The Graphene bilayer has attracted a lot of interest in particular. Although electrons generate chiral excitations, as in monolayer Graphene the electrical interaction between the layers generates a quadratic energy-momentum dispersion, allowing large Dirac quasiparticles to function. Because an external electric field can induce a controlled gap to open, as was recently proven for exfoliated Graphene on a Silicon Di-oxide substrate, this technology is highly interesting for future applications [41, 42].

The translations and twisting of the constituent layers are the structural degrees of freedom of few layer Graphene. While the electronic implications of the first degree of freedom have long been investigated, the rotational degree of freedom has only recently gained popularity. The discovery by Hass et al. [43] that Graphene grown epitaxially on SiC $(000\bar{1})$ contains a high density of twist boundary faults, i.e. layers with a relative twist, has sparked this interest. They also showed that a two layer structure with a common relative twist (cos=30°$\pm$2:20°) exhibits an apparent electronic decoupling. Namely, ab initio computations proved that both layers showed the Dirac cone and Fermi velocity characteristic of monolayer. This remarkable result has inspired a number of subsequent theoretical and experimental work [43-45]. In Ref. [45], Ab initio computations were used to explore bilayer and tri layer twist boundary systems, and layers with a relative rotation were found to exhibit apparent monolayer behaviour in both situations. On the other hand, Ref.[43] In comparison to monolayer, the limit $\theta \rightarrow 0$ of the rotating bilayer was examined in a continuum approximation, with the result that the layers

were perfectly decoupled but the Fermi velocity of the Dirac cone was subdued. This latter finding contrasts sharply with ab initio estimates[45, 46] for finite twisting angles, a Fermi velocity that is exactly equal to monolayer is discovered.

Since only certain rotation angles or restrictions have been explored to date, the details of the entire set of twisting angles that produce decoupling remains an open subject. The basic physical process with lying this dissociation, which is still unknown at this point, is also of great interest. They have shown in this paper that all finite twisting angles that produce commensurate structures result in approximate, but almost perfect, decoupling, with precise decoupling occurring only in the limit $\theta \rightarrow 0$ or for incommensurate rotations. We find a destructive interference between the layers as the cause of this extraordinary behaviour, which can be described by a reciprocal space commensuration condition.[40].

Since only certain rotation angles or restrictions have been explored to date, the identity of the entire set of rotation angles that produce decoupling remains an open subject. The basic physical process with lying this dissociation, which is still unknown at this point, is also of great interest. We show in this paper that all finite rotation angles that produce commensurate structures result in approximate, but almost perfect, decoupling, with precise decoupling occurring only in the limit 0 or for incommensurate rotations. We find a destructive interference between the layers as the cause of this extraordinary behaviour, which can be described by a reciprocal space commensuration condition. This condition can be stated as follows:

$\mathbf{a}_2=\mathbf{R}\mathbf{a}_1$, with $\mathbf{a}_{1,2}$ direct-lattice vectors and $\mathbf{R}$ is the rotation operator. This condition is written in natural lattice coordinates as:

$$\begin{pmatrix} m_1 \\ m_2 \end{pmatrix} = T^{-1} R T \begin{pmatrix} n_1 \\ n_2 \end{pmatrix} \tag{2}$$

T is the transformation operator between the triangular lattice and Cartesian coordinate systems. Because both m and n are integer-valued in the lattice coordinate system, Eq. (2) is a Diophantine system that may be represented as with a standard set of basis vectors.

$$\begin{pmatrix} m_1 \\ m_2 \end{pmatrix} = \begin{pmatrix} \frac{1}{\sqrt{3}}\sin\theta + \cos\theta & \frac{2}{\sqrt{3}}\sin\theta \\ -\frac{2}{\sqrt{3}}\sin\theta & -\frac{1}{\sqrt{3}}\sin\theta + \cos\theta \end{pmatrix} \begin{pmatrix} n_1 \\ n_2 \end{pmatrix} \tag{3}$$

The matrix must be rational-valued in order for this problem to have an integer solution, which indicates that $\cos\theta = i_2/i_3$ and $\sin\theta/\sqrt{3} = i1/i3$ and so $3(i_1)^2 + (i_2)^2 = (i_3)^2$,

where $\{i_1, i_2, i_3\} \in Z=$

Solution of this Diophantine equation is therefore

$i_1=p^2-2pq-3q^2$ (3)

$i_2=-(p^2+6pq-3q^2)$ (4)

$i_3=2(p^2+3q^2)$ (5)

and as a result, the issue is simplified to a set of Diophantine equations for unknown integers n_1, n_2, m_1, and m_2.

These equations contain infinitely many solutions for any (p,q) pair, which correspond to two superlattices of sites connected by Eq (2). A (p,q) integer pair can thus be used to designate every commensuration of two Graphene layers. The only thing left is to find the primitive commensuration cells from these superlattices.

Defining δ=3/gcd(p,3), we find for δ=1.

$\mathbf{t}_1=\frac{1}{\gamma}(p+3q)\boldsymbol{a_1} + \frac{1}{\gamma}(p-3q)\,\boldsymbol{a_2}$ (6)

$\mathbf{t}_2=-\frac{1}{\gamma}(2p)\boldsymbol{a_1} + \frac{1}{\gamma}(p+3q)\,\boldsymbol{a_2}$ (7)

and for δ=3

$\mathbf{t}_1=\frac{1}{\gamma}(p+q)\boldsymbol{a_1} - \frac{1}{\gamma}(2q)\,\boldsymbol{a_2}$ (8)

$\mathbf{t}_2=-\frac{1}{\gamma}(p-q)\boldsymbol{a_1} + \frac{1}{\gamma}(p+q)\,\boldsymbol{a_2}$ (9)

Where γ =gcd (p + 3q, p - 3q). The commensurations found in Ref. [43] are a specific instance of the ones provided here; they can be recovered through the use of the choice method (p,q)=(1,2*i*+1) and for which always γ=2 and δ=3. A more convenient formulation of the rotation angle can then be found using these primitive vectors.

$\theta=cos^{-1}\frac{(3q^2-p^2)}{(3q^2+p^2)}$ (10)

(it is defined so that for $p \geq q$ we have $0 < \theta < \pi/3$), and in the commensuration cell, the number of primitive vectors in each layer

$$N=\frac{3}{\delta}\frac{1}{(\gamma^2)}(3q^2+p^2) \quad (11)$$

4N is the number of carbon atoms in the cell. This multiplier of four is related to the fact that the cell has two layers and the honeycomb structure has two basis atoms. The rapidly increasing sequence described by Eq. (11) as $\theta \rightarrow 0$ [$4N = (\sin^2\theta/2)^{-1}$ is ab initio computations for the entire range of angles are prohibitively expensive due to the lower bound. Fortunately, as we will see, it is easy to make a broad statement about the angular dependency of the electrical coupling. [43].

1.5 Motivation of Thesis

The motivation of the thesis work is to analyzed effect interlayer twist angle on the electronic structure of Homobilayer of $MoSe_2$ and 2D heterostructure of $GaTe/MoS_2$ structures. From the discovery of Graphene, in 2004, a lot of research going on monolayer properties of 2D materials. However, there is lot of issue associated with monolayer, such as high contact resistance, not suitable doping technique etc. As compare to monolayer, homo bilayer of 2D semiconductors, also explored due to high capacity of carrying current, good mobility and lower contact resistance. On the hand, the 2D heterostructures also explored by research community due to availability of various degree of freedom of tuning of the structure. Therefore, In this thesis we have a taken interlayer twist angle to modulated the electronic structure and optical properties of 2D materials for their possible application in optoelectronics.

1.6 Organization of Thesis

We have organized this this Thesis in the following manner:

1. The first chapter is about introduction of 2D materials community. Particularly, the 2D semiconducting materials such as TMDCs materials discussed in the details. Basic details of DFT theory also introduced in brief manner. Further, we discussed in the

details the concept of Twistronics. The basic fundamentals of magic angle discussed in the details. The mathematically modelling of interlayer twist angle is discussed in the details. Finally, Motivation and organization of thesis is discussed in the detail.

2. In the second chapter, the literature review about 2D materials, it heterostructure, the effect of twisting on Homobilayer and heterostructure studied in the details.

3. In the third chapter, the electronic structure and optical properties of AB stacked 2L $MoSe_2$ with various interlayer twist angle discussed in the details. The band structure, projected density of states (PDOS), optical spectra and electron localization function (ELF) discussed in the details.

4. In the fourth chapter, we have discussed the formation and stability of 2D heterostructure based on the GaTe and MoS_2 monolayer with different possible stacking order. Here we have focused on the most stable vertical stacking order.

5. In the chapter five , we have analyzed the electronic structure and optical properties GaTe/MoS_2 heterostructure at various interlayer twist angle. Basically we have estimated the electronic and optical properties at various interlayer rotation angles and how these properties are being changed with different twist angles.

6. Finally in the conclusion which is chapter sixth ,we have discussed about the research implications and future scopes.

Chapter 2

Literature Review

2.1 Introduction

Since discovery of Graphene in 2004, the field of 2D Materials has advanced tremendously,[47] . Further, the Nobel Prize for Physics was also awarded in 2010 Graphene is often regarded as the first isolated 2D substance. Hundreds of stable monolayer materials have been predicted, and several monolayer materials with a variety of chemistry and crystal structures have been produced. Hexagonal boron nitride (hBN- widely used in glass manufacturing process), TMDCs, Xenes (here X = Si, Ge, Sn,...), MXenes, and Chromium Tri-halides are examples of these materials. Various types of sensors such as Optical sensors, biosensors, chemical sensors, strain sensors, , injection of spin current, massless resonators, neural interfaces, neural scaffolds, single ion detection, DNA/RNA sequencing, protein characterization, low-cost organic solar cells, single photon emitters, Light Emitting Diodes (LED) , superconductivity, transistors, piezoelectric, and magnetism are just a few of the fields where monolayer materials have made a difference.

Although a perfect definition of 2D materials has yet to be established, most 2D materials are few-atom thick, and their properties can be described by quasi particle excitations confined in two dimensions (i.e., their band structure has two momentum dimensions, k_x and k_y, and one energy dimension, with the nth band described by $E_n = E_n(k_x, k_y)$), and chemically, their surface bonds are completely satisfied (i.e. they do not have unsatisfied surface dangling bonds). Because of this, it's safe to assume that single layers of these materials have strong in-plane bonding and poor out-of-plane bonding. This gave rise to the concept of van der Waals (vdW)

layered solids, a new type of pseudo-crystalline solid created by vertical stacking of 2D materials[48].

2.2 Review on two-dimensional homo and heterostructure with twist angles

Initially we have focused on the review literature of homo bilayer and heterostructures.

In 2008 Shallcross *et al.* [53] Density functional theory is used to explore the energetics of Graphene layers' translational and rotational degrees of freedom. The sliding (translation) energy of a bilayer is discovered to be highly dependent on whether or not the layers are mutually rotated. While the sliding energy of unrotated layers is high, the sliding energy of mutually rotated layers is zero, with the AB stacked bilayer having the lowest energy. When we look at the rotational degree of freedom, we see that energy is highly dependent on the relative rotation between layers, with $30^{\circ} \pm 2.208^{\circ}$ generating the lowest energy structure.

In 2014, Zhao *et al.*[51] using first-principles computations analyzed two alternative models of Graphene and h-BN from the viewpoints of lattice match and lattice mismatch.

In 2019, Zhang *et al.* [49] found that by twisting two single layers, the band gap type of bilayer WSe_2 can be changed from indirect to direct. With six twist angles, the external electric field can enable the bilayer WSe2 to achieve a semiconductor to metal transition. The stacking configurations of 0° and 60° in particular display transport anisotropy, with the zigzag route transporting slightly better than the armchair direction. Furthermore, when an external electric field is applied, the transport performance of the case with twisted 60° is superior than that of the case with 0°, regardless of the edge orientation. This findings pave the way for future WSe2-based microelectronics and optoelectronic devices to be designed and used.

In 2020 W. T. Geng *et al.* [54] revealed that because the interlayer overlapping degree increases with increasing twist angle in a twisted $MoS_2/MoTe_2$ heterobilayer, the interlayer binding decreases, a geometric number that accurately describes the interlayer steric effect. It is discovered that the binding energy is a Gaussian-like function of twist angle. The rotational resistance, which is analogous to the interlayer sliding barrier, can also be characterised in this way. In contrast to the MoS_2 homobilayer, the energy band gap here decreases as the twist

angle increases. They found that the band gap is widened by a spectacular interlayer charge transfer from MoTe2 to MoS_2, but this charge transfer reduces as the twisting and interlayer overlapping degree increases. Our discovery provides a solid foundation in twistronics as well as practical education in van der Waals heterostructure band structure engineering.

Recently, in 2021 Innocent Joseph *et al. [50]* reported the electrical structures and optoelectronic properties of the BP-MoS_2 vdW heterostructure as a function of interlayer rotation angle. They discovered that the heterostructure has tunable band alignment across type I and II with adjustments in interlayer rotation angle in the range of 0–60. Specifically, type II BP- MoS_2 vdW heterostructures with rotation angles of 0 to 60 were projected to have a considerable potential drop across the interface to separate photoinduced-charge carriers, which is critical for photovoltaic and photocatalysis applications.

In 2021 Xiaojing Yao *et al.* [55] Using first-principles calculations, researchers investigated the structures and electronic characteristics of twisted bilayer InSe/InSe and heterobilayer Gr/InSe. Due to spontaneous polarisation between two InSe layers, the band structures of AB-stacking InSe/InSe differ from their twisted isomers for bilayer InSe/InSe, but the twisted systems have nearly similar band gaps. The band gaps of the twisted Gr/InSe heterostructure change depending on the interlayer misorientation angles.

Most recently in this year 2022, Yonghao Zhu *et al.* [56] found that in the MoS_2/ WS_2bilayer, twist angle has a minor affect on charge separation but a substantial influence on recombination. Van der Waals heterojunctions of two-dimensional transition-metal dichalcogenides are extensively researched in this research study for a variety of optoelectronics applications. The charge and energy flow that regulate material performance can be influenced by strong and tunable interactions between layers.

Interlayer distance changes, electron-vibrational interactions, and out-of-plane vibrational frequency spectrum shifts all show that the twist angle impacts interlayer coupling. The hole transfer, which takes place on a femtosecond timescale, is ultrafast because to the high density of acceptor states and significant nonadiabatic coupling. The electron–hole recombination, on the other hand, takes nanoseconds and depends on the twist angle by an order of magnitude.

Because it occurs across a wide energy gap, recombination is sluggish. The twist angle is reliant on the nonadiabatic coupling because it is sensitive to the interlayer distance and overlap of electron and hole wavefunctions. Interlayer contact is weaker in Moiré pattern systems, resulting in longer-lasting charges. Charge separation and recombination are both fueled by out-of-plane vibrational motions. The simulations explain the experimental findings on the effect of bilayer twist angle on charge separation and recombination. Theoretical direction for the construction of high-performance optoelectronic devices based on two-dimensional van der Waals heterostructures is provided by the atomistic insights.

Chapter 3

Electronic structure evaluation and optical properties of bilayer $MoSe_2$ with various twist angle

3.1 Introduction

Even though TMDCs have been investigated for decades, recent advances in nanoscale materials characterisation and device manufacturing have made 2D layers of thin TMDCs are more promising for nanoelectronics and optoelectronics Therefore, in this chapter, we have taken bilayer of $MoSe_2$ with AB stacking order to study effect of interlayer twist angle on the electronic structure and optical properties.

3.2 AB stacked bilayer (2L) $MoSe_2$

In AB stacked 2L $MoSe_2$, the Mo atoms at the 2^{nd} monolayer surface lie vertically above the Se atoms at the 1^{st} monolayer surface in AB stacked bilayer $MoSe_2$, as shown in Fig. 3.1. As compare to AA stacking, AB 2L $MoSe_2$ stacking has a 40 meV lower energy, making AB stacking more advantageous in energy perspective. Therefore, for further calculations, we have taken AB stacking into account.

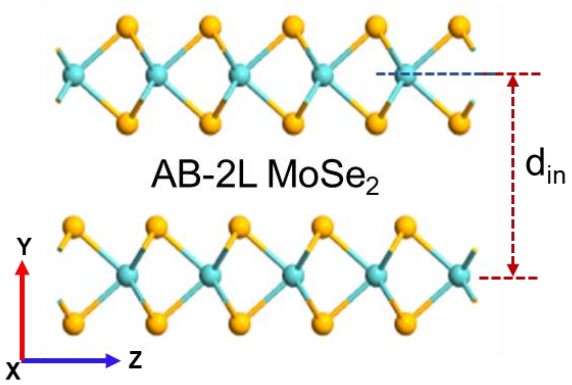

Figure 3.1 Schematic atomic structure of 2L $MoSe_2$ with AB stacking order

3.3 Computation details

DFT Calculations: Density functional theory (DFT), which is implemented in the Quantum Atk, is used to calculate the electronic band structure and transport parameters of bilayer $MoSe_2$. Within the generalised gradient approximations of the PerdewBurkeErnzerhof exchange correlation functional, the Quantum Atk is employed in conjunction with the linear combination of atomic orbitals (LCAO) approach. The SG15[49] pseudopotential is used to expand the electron wave function, and the basis set is precisely determined. All computations were performed with a density mesh cutoff energy of 180 hartree. The Monkhorst Pack -point grid of 16×16 ×1, 6× 6× 1, 6× 6× 1 and 16×16 ×1 is used in the calculations for different twist angles of 0°, , 21.79°, 38.21°, and 60°, respectively, to ensure the bilayer $MoSe_2$ has the same sampling density with different twist angles in the reciprocal [49] The strain induced by the lattice mismatch is zero during the process of twisting two single layers to obtain six rotation angles. The long-range vdW coupling will be addressed using a semi-empirical Grimme adjustment , which focuses on the impact of the interaction on the DFT mean-field effective potential rather than the actual source of the interaction (fluctuating dipoles).The DFT-D2 functional exploited by Grimme[49] augments that to account for vdW coupling, or dispersion forces, an extra component of the DFT total energy is added. However, due to the incompleteness of the LCAO basis set, the interlayer distance between two single layers is not sufficiently accurate if the Grimme correction is used without taking the basis set superposition error (BSSE) into account. To process the BSSE of LCAO basis sets, we used the Grimme DFTD2 semi-empirical correction as established in the ATK ,mix with the counterpoise

correction to consider the vdW coupling in the bilayer $MoSe_2$ [59-61]. To model bilayer $MoSe_2$, a unit cell with a periodic boundary condition was used. The layered structures are on the xy plane, with a vacuum thickness of 16 used to prevent interaction between periodic slab images in the z direction. The limited-memory algorithm optimises the geometric structures. [62] The final force applied on each atom in the optimised structure is less than 0.01 eV/Å for each ionic step, and the maximal stress tolerance is less than 0.001 eV/$Å^3$

Basis set superposition error (BSSE): The basis set superposition error (BSSE) occurs in polyatomic systems due to the localised nature of the LCAO basis set. Consider a system made up of two subunits A and B to better comprehend the BSSE's origins. Consider each subunit to be a single atom for the sake of simplicity. When A and B are far away, the basis orbitals centred on their respective atomic nuclei are all that exists to characterise them. When A couples to B, however, the basis functions centred at A and those centred at B overlap. As a result, A can be described using a portion of the basic orbitals centred at B. This creates a fictitious attraction between A and B. Fig. 3.2 shows the schematic diagram shows superposition inaccuracy in the basis set's origin.

The BSSE can be made minimum by using the counterpoise correction of energy [58]:

$E=E_{AB}+E^{CP}$

where E_{AB} is the system's total energy AB and **E** is counterpoise correction of energy.

The counterpoise correction of energy is obtained through:

$E^{CP}=(E_A- E_{AB'})+(E_B-E_{A'B})$

where E_{AB}' is the energy of system A in the AB basis, which is determined by characterising the atoms of B as ghost atoms and getting the entire system to its equilibrium geometry While ghost atoms have no charge or mass, they do have basis orbitals, which are determined by the element (and basis set) that would normally characterise the atom.

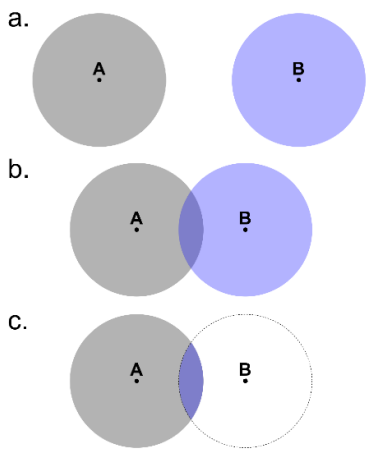

Figure 3.2 The superposition inaccuracy in the basis set's origin. (a) A and B are far away; (b) when A couples to B, basis orbitals overlap; (c) the blue zone denotes the fraction of the basis orbitals centred at B that can be used to characterise A.

The counterpoise adjustment can easily be applied to a large number of subunits, Ai, through:

$E^{CP}=\sum_i \{E(Ai) - E(AiCi')\}$

where Ci is the Ai complement, i.e. the atoms not in region Ai.

We must alter the definition of the Calculator in the Editor to add BSSE correction. Steps to be followed in Quantum ATK to perform BSSE correction:

1. **Set up the $MoSe_2$ bilayer system –** Change the C-length vector's to 16 Å in builder. The $MoSe_2$ crystal becomes a bilayer $MoSe_2$ model as a result of this transformation. Then, using Coordinate Tools - Center, centre the shape. Each $MoSe_2$ layer must have a tag added to complete the structure configuration. In order to define the counterpoise correction, tags are utilised to distinguish the two layers. Select the two atoms in the first $MoSe_2$ layer, open Selection Tools Tags, and type "layer1" in the bottommost area to add the tags. Then repeat the process for the second layer, labelling it "layer2."
2. Optimization of geometry without counterpoise correction
3. Examine the Improved Structure
4. Taking into account the counterpoise adjustment
5. Taking into account the D2 dispersion correction

```
#calculator = LCAOCalculator(
#    basis_set=basis_set,
```

```
#    exchange_correlation=exchange_correlation,
#    numerical_accuracy_parameters=numerical_accuracy_parameters,
#    correction_extension=correction_extension,

#    )

#BSSE CP correction

bsse_calculator = counterpoise Corrected (LCAOCalculator, ["Layer1" , "Layer2"])
calculator = bsse_calculator(
    basis_set=basis_set,
    exchange_correlation=exchange_correlation,
    numerical_accuracy_parameters=numerical_accuracy_parameters,
    correction_extension=correction_extension,
    )
```

3.4 Results and discussion

3.4.1 Atomic structure with various twist angle

Twisting two monolayer $MoSe_2$ layers with respect to each other gives twisted 2L $MoSe_2$ structures with various rotation degrees. Simultaneously, the supercells at various rotation angles are geometrically optimised to acquire the optimum lattice constants, with the smallest lattice mismatch and number of supercell atoms. The schematic diagram of AB stacked 2L $MoSe_2$ with various twist angles are shown in Fig. 3.3 (a)-(d). Clearly, at 0° and 60° has smallest number of atoms (6). When interlayer of 2L $MoSe_2$ twisted at 21.79° and 38.21°, the number of atoms increases. In this study, we have limited number of atoms less than 100 atoms due to limited computation efficiency. We have taken all the commensurate structure at different angles while keeping the strain / lattice mismatch 0 %. By taking into account BSSE corrections, we have also calculated interlayer distance with every twisting angle as shown in Table. 3.1. It is clear, that with twisting interlayer distance increases and it is highest at 60°.

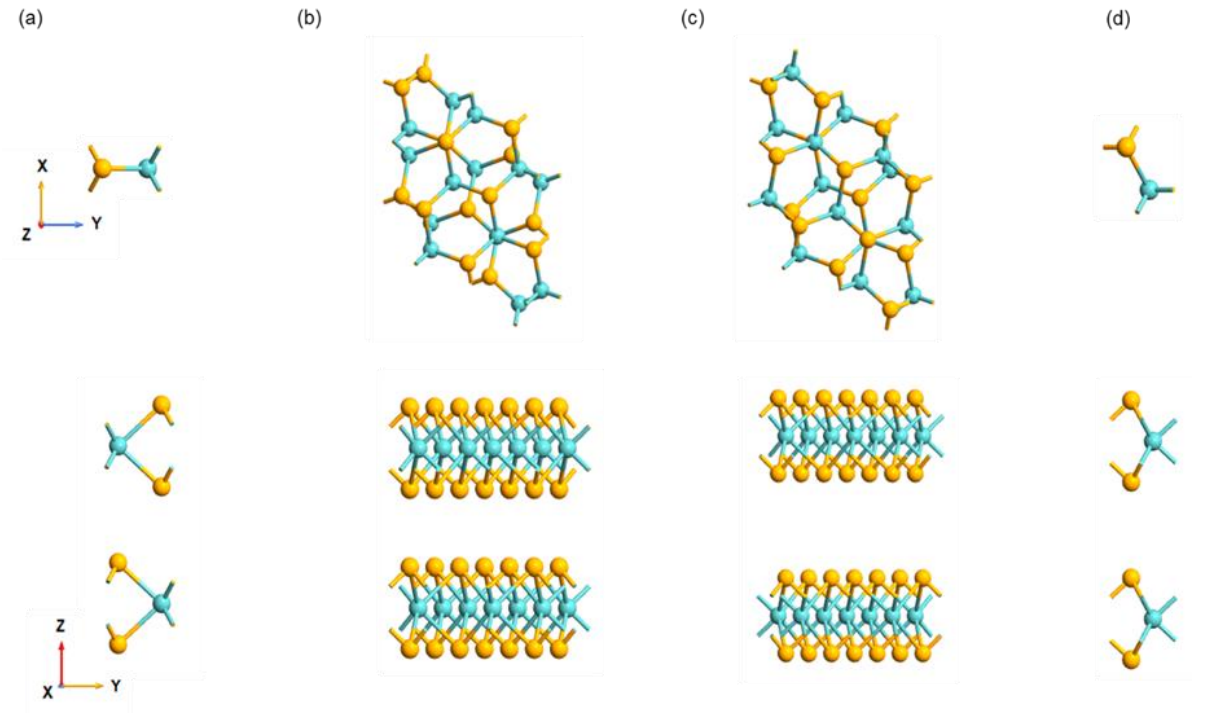

Figure 3.3 Top and side view of bilayer $MoSe_2$ with different twist angles of (a) 0°, (b) 21.79°, (c) 38.21°, and (d) 60° respectively.

3.4.2 Band structure and Projected Band structure with various twist angle

Now, we have analyzed band structure of 2L $MoSe_2$ with all twist angles. At zero-degree angle, 2L $MoSe_2$ is indirect band gap semiconductor with valance band maximum (VBM) at Γ-point and conduction band minimum (CBM) at K point with band gap value 1.14 eV, well matched with the literature. When we the interlayer twist angle is 21.79˚, then the band gap increases from 1.14 to 1.43 eV, the nature of bandgap transition remain same as 0˚, but the VBM energy and K and Γ point comes very closer, have a difference of the differene of energy between K and Γ point. Further, when interlayer twist increases to 38.21˚, the band gap value remains same as 21.79˚ but nature of band gap changes from indirect to direct. This is very important observations, because it looks like at interlayer twist of 38.21˚, the 2L $MoSe_2$ behaves like monolayer $MoSe_2$ with similar value of band gap. Now, at interlayer twist of 60˚, the band gap value reduces to 1.41 eV, with VBM energy difference at K and Γ point almost similar. This can be well explained by charge and energy transfer during interlayer rotation process.

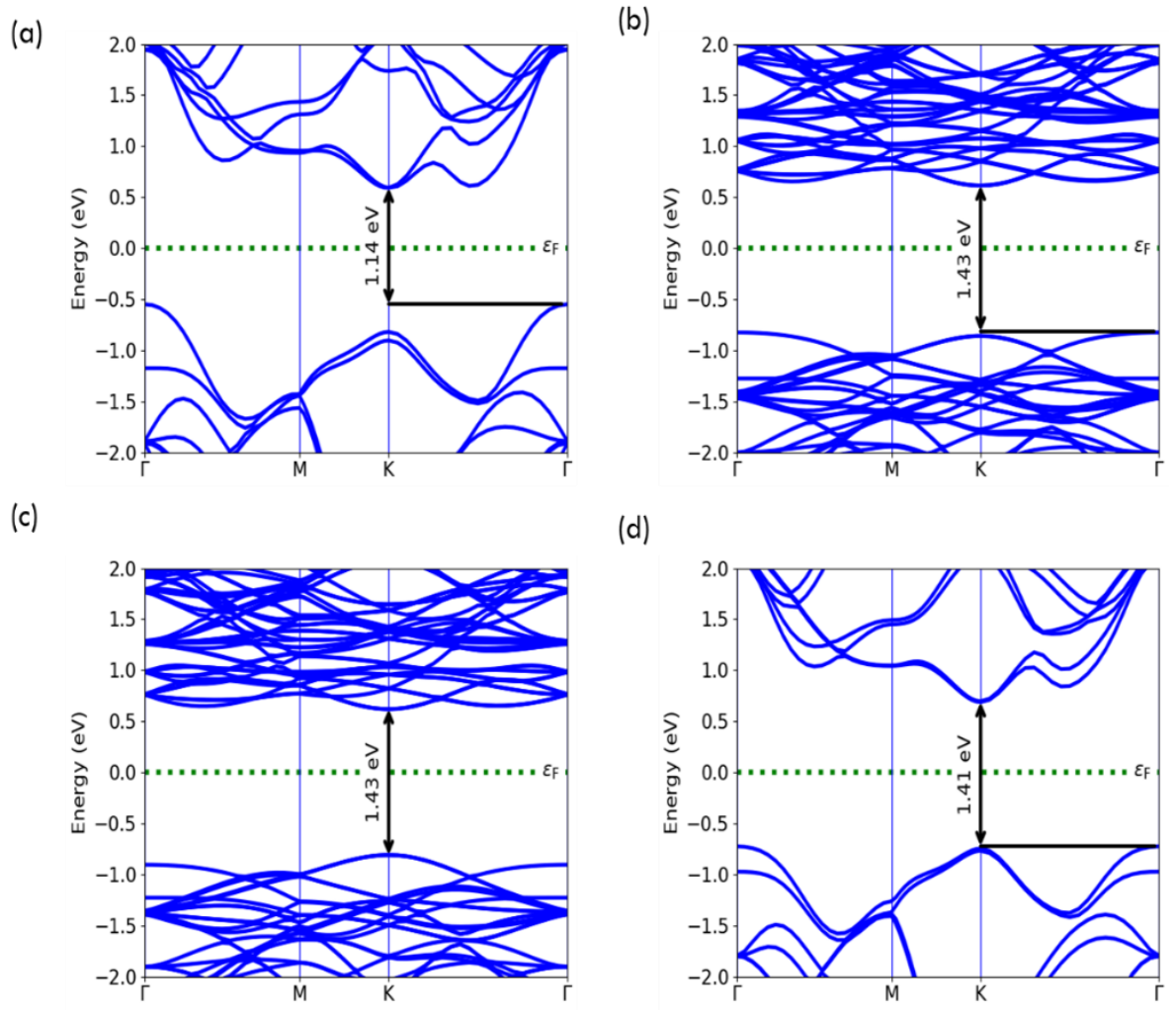

Figure 3.4 Band structure of $MoSe_2$ bilayer with different Twist angle of (a) 0°, (b) 21.79°, (c) 38.21°, and (d) 60° respectively.

Now, the projection of density of states (DOS) at different orbitals are shown in Fig. 3.4. We can see at 0°, the contribution of 4p orbitals from Se atom and 4d orbitals of Mo atom are main in CBM and VBM. When the interlayer twist at 21.79°, the value of DOS increases with contributions remain the same. Further, at 38.21°, the value of DOS decreases and at 60° the value of DOS close to the 0° with contributions of orbitals remain the same.

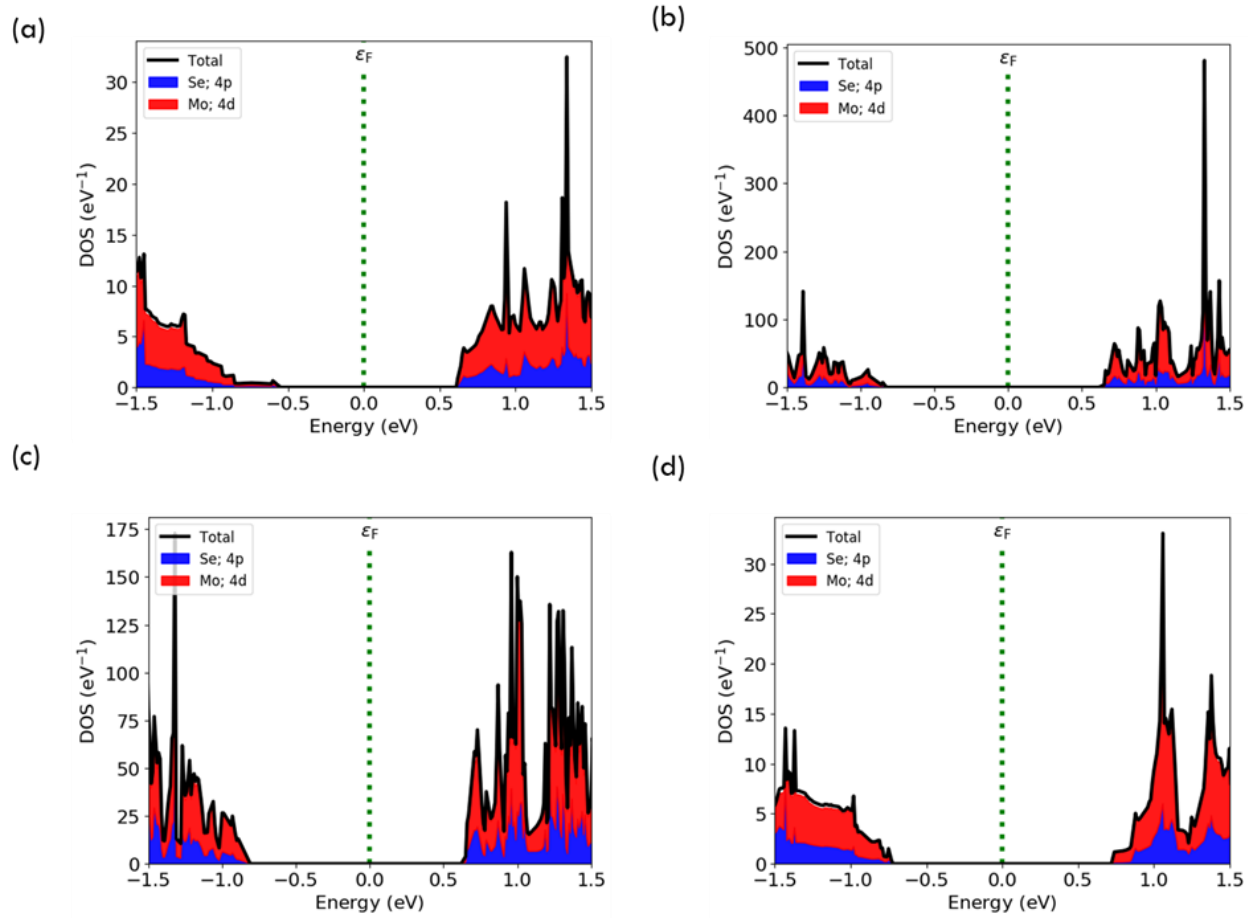

Figure 3.5 Projected Density of States of Bilayer $MoSe_2$ with different Twist angle of (a) 0°, (b) 21.79°, (c) 38.21°, and (d) 60° respectively.

3.4.3. Effect of twist angles on optical properties

Now, we analyses the effect of twist angle on the optical spectrum of 2L $MoSe_2$. The optical spectrum can be calculated from the frequency-dependent complex dielectric function ε (ω) =ε_1 (ω) + ε_2 (ω) is calculated. The energy-dependent absorption coefficient α (ω) can be deduced from ε_1 and ε_2 and mathematically written as

$$\alpha\ (\omega)\ = \sqrt{2}\omega\ [\sqrt{(\varepsilon_1^2(\omega)+\varepsilon_2^2(\omega))}-\varepsilon_1(\omega)]^{1/2} = \frac{2k\omega}{C}$$

where ω is the frequency of light, c is the velocity of light κ is the extinction coefficient. The imaginary part ε_2 (ω) is used to measure the optical absorption in materials and the real part ε_1 (ω) is associated with dispersion in materials deduced from the imaginary part ε_2 by the well-known Kramer−Kronig relation.

The Fig. 3.5 shows the optical spectrum of 2L-$MoSe_2$ with varying twist angles. It is clearly visible that with interlayer twist, the optical spectrum can be modulated. At 0° and 60°, the optical absorption remain the same, with little reduction in the absorption at 60°. Similarly, at 21.79° and 38.21°. the absorption spectra is red shifted with reduction in the absorption.

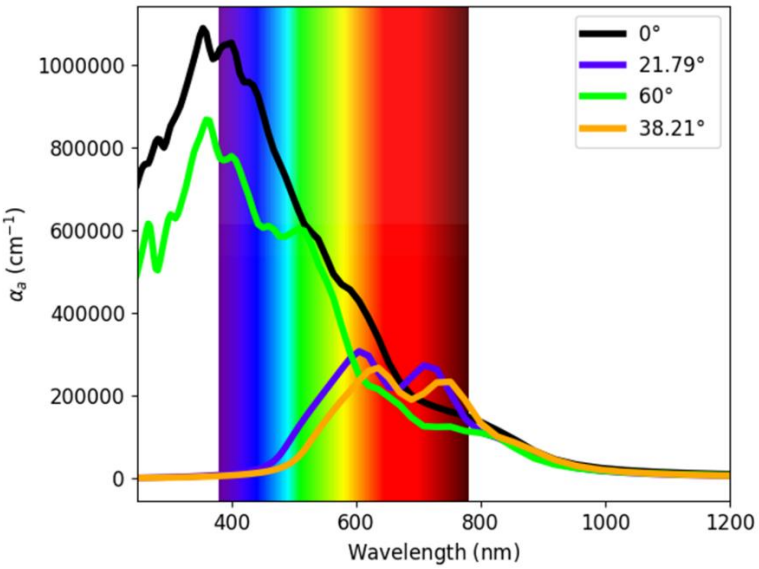

Figure 3.6 Optical Spectrum of 2L $MoSe_2$ with various Twist angle form 0° to 60°.

3.4.4 Electron Localization function (ELF)

The electron localization function (ELF) represents localization of electron in the materials and it is varied from between the range from 0 to 1, whereas ELF = 1 signifies perfect localization of electrons, and ELF= 0 means there are no electrons present in that region or space. Further, the delocalized electron like in an electron gas ("covalent") leads to an ELF = 0.5. [64],. The LCAO Calculator is the sole tool that can calculate the electron localization function. The ELF function of 2L $MoSe_2$ at various interlayer twist angles are shown in Fig. 3.6, it has been made using the cut-plane viewer in Quantum Atk. Clearly, the red zones, green zone, blue zone are representing high electron localization, moderate electron localization and no electron localization respectively. These ELF figures depicts that there is no electron localization between the two $MoSe_2$ layers. The electrons are mostly localized near the surface of each layer.

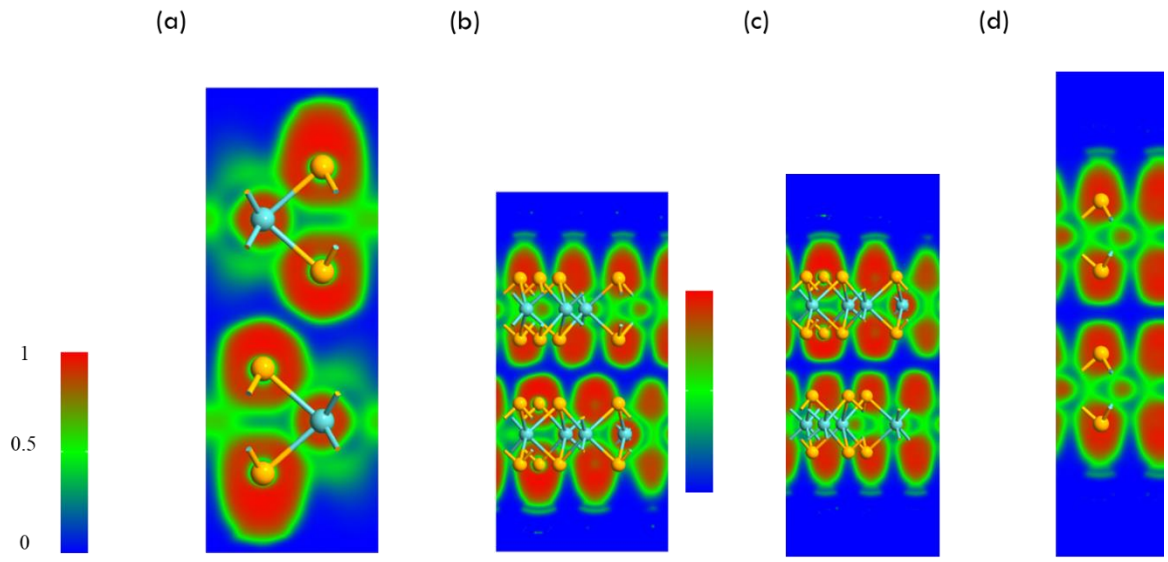

Figure 3.7 ELF of 2L $MoSe_2$ with different Twist angle of (a) 0°, (b) 21.79°, (c) 38.21°, and (d) 60° respectively.

Table.3.1 shows the all the calculated parameters for $MoSe_2$/ $MoSe_2$ homobilayer are various interlayer twist angle.

Rotation Between Surfaces	Lattice Constant (a)	Interlayer Distance	Angle Between Surfaces	No. of atom	Bandgap	Direct/Indirect
0°	3.35	3.15	60°	6	1.14	Indirect
21.79°	8.77	3.55	90°	42	1.43	Indirect
38.21°	8.85	3.81	120°	42	1.43	Direct
60°	3.35	4.01	60°	6	1.41	Indirect

3.5 Conclusion

In this chapter, we have studied 2L-$MoSe_2$ structure with various interlayer twist angles varying from 0°, 21.79°, 38.21°, and 60°. The strain value between the layer is 0 % throughout the work, with number of atoms kept minimum to 100 to avoid larger computational pressure. We observed that, at 0°, the 2L $MoSe_2$ is an indirect band gap semiconductor with bandgap transition route Γ to K. With the interlayer twist increases from 0°, to 21.79°, the different of energy in VBM at K and Γ reduces, the band gap value increases. When the twist angle is 21.79°, the VBM energy at K point increases as compare to Γ, the band gap become direct in nature with band gap value equal to 1.43 eV. The behaviour of 2L $MoSe_2$ at 38.21° is similar it monolayer $MoSe_2$, which suggest that with suitable twist angle the 2L $MoSe_2$ can be utilized as direct band gap materials in several electronic and optoelectronics applications. Further, by varying twist angle, the optical absorption also vary, although, the no localization of electrons between the interlayer observed.

.

Chapter 4

Formation and stability of two-dimensional GaTe/MoS_2 heterostructure

4.1 Introduction

Individual 2D monolayer layers in vdW heterostructures can have strong coupling and hence diverse electronic structures, which makes them a better candidate in electronic and optoelectronic applications. In this chapter, we studied formation and stability of GaTe/MoS_2 vdW heterostructure using DFT computations First, we relax and optimized, the stacking order of 2D GaTe/MoS_2 heterostructure using binding energy calculations.

4.2 Computation details

The DFT calculations were carried out employing the Virtual Nano lab Quantum-ATK. The exchange-correlation functionals were described within generalized gradient approximation (GGA) in the Perdew–Burke–Ernzerhof (PBE) form with an energy cut-off of 125 Hartree. The Brillouin-zone integrations were performed with Monkhorst-Pack k- points with a grid sampling of 5 × 5 × 1. Structures were fully relaxed to minimize the system's total energy until the force on each atom is less than 0.01 eV/Å. The van der Waals forces are taken into account by using a Grimme DFT-D2 dispersion-correction approach. A vacuum space of 22 Å is included perpendicular to the surface to eliminate the coupling between neighbouring cells.

4.3 Results and discussion

4.3.1 Electronic Structure of GaTe and MoS_2 monolayer

The hexagonal lattice of the GaTe monolayer contains a Te–Ga–Ga–Te sequence repeating unit via covalent bonds, and the estimated lattice parameters are a = b = 4.1346 Å. The Te–Ga and Ga–Ga bond lengths are $d_{Te\text{-}Ga}$ = 2.71 and $d_{Ga\text{-}Ga}$ = 2.47, respectively, which are consistent with earlier theoretical and experimental results[67]. Before making the GaTe/MoS_2 heterostructure we have first analyzed both the GaTe monolayer and MoS_2 monolayer. We have observed the monolayer GaTe has Indirect band gap of 1.46 eV as shown in Fig.(c),which is very close to the reported band gap (1.4 eV) [68].

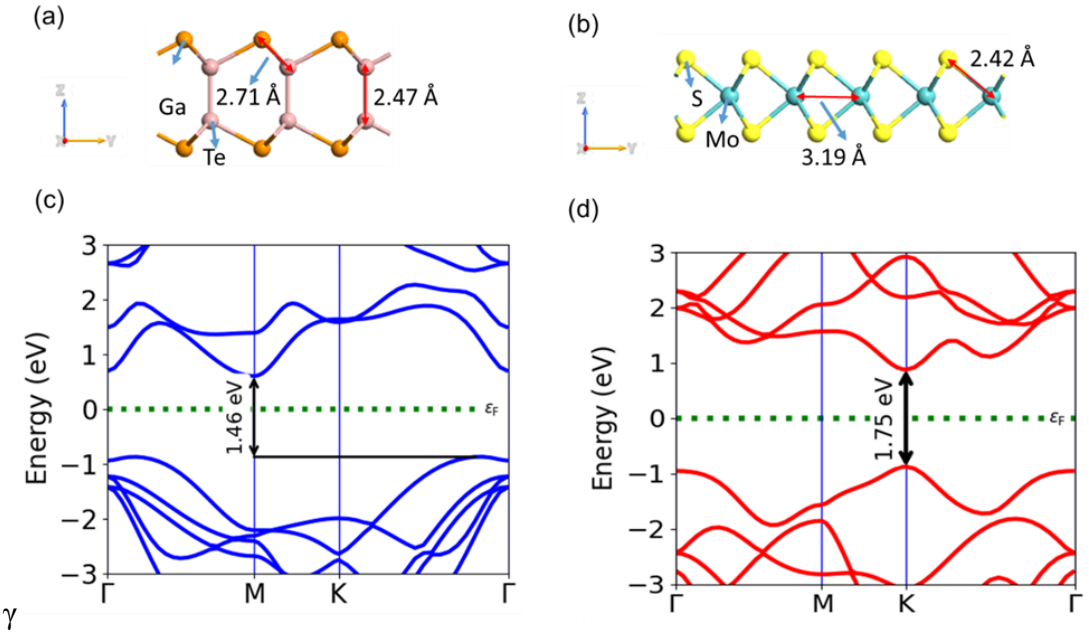

Figure 4.1 (a) Electronic Structure of GaTe monolayer, (b) Electronic Structure of MoS_2 monolayer, (c) Band structure of GaTe monolayer, (d) Band structure of MoS_2 monolayer

The bulk MoS_2 crystal is having indirect band gap of 1.29 eV [69]. But for the MoS_2 single layer, it has a direct band gap of 1.75 eV (Fig. d) which is forming from both the CBM and VBM at the *K* point.This band gap is close to the band gap reported by Mak et al. [70]. The intra layer atoms in the MoS_2 single layer are sandwiched in the order S–Mo–S, which represents hexagonal configurations. MoS_2 has lattice constants of a = b = 3.13696 Å , which are consistent with published research[71].

4.3.2 Formation of $GaTe/MoS_2$ structure

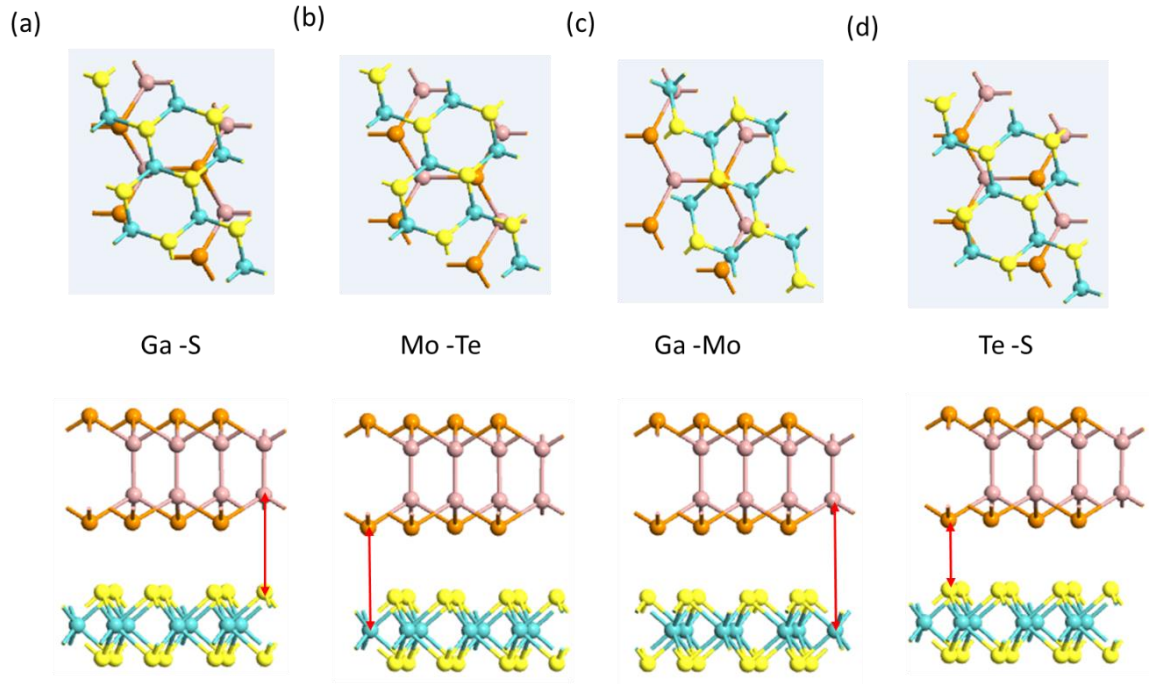

Figure 4.2 (a) AB Stacking where Ga atom is at the top of the S atom (b) AA Stacking where Te atom is at the top of the Mo atom (c) $A\bar{A}$ Stacking where Ga atom is at the top of the Mo atom (d) $A\bar{B}$ Stacking where Te atom is at the top of the S atom

We can form four possible heterostructure for $GaTe/MoS_2$ because here we have four different atoms.. In the above figures we can see the four combination. In order to discuss the consequences of stacking patterns in the $GaTe/MoS_2$ vdWH, four different stacking configurations are considered, as illustrated in the diagram above. The Ga atom is found at the top site of the S atom, while the Te atom is found at the top site of the Mo atom. The Ga atom is found at the top site of the Mo atom, while the Te atom is found at the top site of the S atom. We named these different stacking orders as AB (Fig. a), AA (Fig. b), $A\bar{A}$ (Fig. c), $A\bar{B}$ (Fig. d). All the configurations are completely relaxed. Both GaTe and MoS_2 single layers appear to retain their native structures without considerable distortion. We estimated the binding energies E_b between the GaTe and MoS_2 single layers to assess the relative structural stability of $GaTe/MoS_2$ vdWH.

4.3.3 Calculation of Binding energy of different stacking order

The binding energy of GaTe/MoS_2 heterostructure is calculated by using the following formula Binding energy, $E_b = E_{GaTe/MoS2} - (E_{GaTe} + E_{MoS2})$

Where $E_{GaTe/MoS2\ b}$ is the total energy for the GaTe/MoS_2 heterostructure, $E_{GaTe\ is}$ the total energy and E_{MoS} is the total energy for MoS_2. All the calculated value of Eb is listed here in the following table. It is clear that the formation of heterostructure is exothermic reaction and it is thermodynamically stable process. From the above table it is clear that the in AB Stacking (Ga atom above the S atom) we have minimum binding energy. So the AB stacking GaTe/MoS_2 heterostructure is the most stable and due to this for further analysis we have used this stable structure throughout the paper to apply various Twist angle.

Stacking Order	Binding Energy (eV)
AB	-1.87
AA	-1.868
$A\bar{A}$	-1.863
$A\bar{B}$	-1.865

4.4. Conclusion

In this chapter, we have calculated the band structure, and DOS of individual monolayer GaTe and MoS_2 monolayer. Then the 2D heterostructure is formed by placing on monolayer on top of each other. Then we have formed the GaTe/MoS_2 Heterostructure with different stacking order to identify the most stable stacking for further analysis. To select the most stable structure we have calculated the binding energy and the structure with least binding energy is the most stable one. All the analysis of this chapter is at 0° Twist angle that means we have not applied any twist in the interlayer. So, this analysis have made our foundational withstanding of heterostructure without the effect of Twistronics

Chapter 5

Electronic and Optical properties of $GaTe/MoS_2$ heterostructure with various Twist angles

5.1 Introduction

After investigating monolayer or single layer materials in their natural state, the next logical step was to arrange them vertically to generate 2D heterostructures. Although, it quickly became clear that the properties of such a 2D heterostructure are not simply a physical positioning of those of its constituent surfaces, though a complicated result of coupling between the surfaces, reconstruction of lattice, and twisting angle, that can express and spawn unanticipated new phenomena. (that the stacking order, or how the lattice points are placed on top of each other even in untwisted self-similar 2D monolayers, can affect the properties of the resulting heterostructures, The angle of twisting (i.e., the relative angle between layers)[26] which determines the new periodicity (i.e., moiré pattern) created between particular crystalline layers, whereas interlayer coupling determines the degree of electron-particle interactions[77] hybridization, charge redistribution, [35] and lattice reconstruction. These elements combine to generate a 2D moiré superlattice with a unique band structure, which results in new properties.

As discussed in chapter 3 of this thesis, the AB stacked $GaTe/MoS_2$ structure is the most stable. In here we have applied various twist angle to observe the different changes. Specifically, we

have applied six different angle for twisting the hetero bilayer of GaTe/MoS_2 and the angles are 0°, 10.89°, 19.11°, 40.89°, 49.11°, 60°.

5.2 Computation details

Quantum ATKs builder interface was used to develop the GaTe/MoS_2 heterostructured models. In order to successfully deal with the geometry of lattice matching and mismatching interfaces in the modelling of innovative vdW heterostructures, one widely used method was to look for a supercell with the least strain in each of the incommensurate single layers. The lattice constants of GaTe and MoS_2 were nearly identical (0.24 % to 0.77 %), and the first heterostructure form was aligned using a zero-degree interlayer rotational angle. We assumed that within a tolerance of, 1×10^{-6} the range of angles between the two surfaces was equivalent, and that the minimum strain developed in the supercell was equal to that of the aligned system. To compensate for the twist angle in other supercells with a twist angle greater than 0° and minimise the effect of artificially created strain in the supercells, an increased number of atoms was considered necessary. On the basis of the base vector in the heterostructure, the corresponding twist angle between GaTe/MoS_2 contacts may be calculated as reported by [51, 78, 79]is expressed as follows:

$t_1=na_1+ma_2$

$t_2=pb_1+qb_2$

$$\cos\theta = \frac{\mathbf{t}1.\,\mathbf{t}2}{|\mathbf{t}1| \times |\mathbf{t}2|} = \frac{np+mq+(nq+mp)/2}{(\sqrt{m*m+mn+n*n})\times\sqrt{p*p+pq+q*q}}$$

Quantum ATK was used to with take computational investigations based on the first principle. The electron exchange correlation was described using the PBE functional with the GGA. The DFT-D2 approach of Grimme and dipole moment correction in parallel direction to the lattice vectors for slab were used to account for the vdW interaction and dipole correction energy in all simulations. Cut off energy of 125 Hartree was set and a vacuum of 22.5Å was used to

prohibit artificial neighbor slab interactions. The convergence condition of the energy and EDIFFG were set as $1 \times 10-5$ eV and 0.001 eV $Å^{-1}$, respectively. Additionally, k-grid of $9 \times 9 \times 1$ for GaTe and MoS_2 single layers was selected and k-grid of $5 \times 5 \times 1$ has been selected for GaTe/MoS_2 heterostructure. Force tolerance was set to 0.01 eV/Å the Stress error tolerance has been set to0.001 eV/$Å^3$. The heterostructure's stability was determined utilising the interlayer binding energy per unit area (E_b) for each supercell and calculated using Eq. ():

E_b (per unit area) = ($E_{GaTe/MoS2}$ –E_{GaTe}-E_{MoS2})/area

Here, $E_{GaTe/MoS2}$, E_{GaTe}, and E_{MoS2} are total energy of heterostructures, composed of monolayers of GaTe and MoS_2, respectively. The charge density differences ($\Delta\rho$) which track charge transfer and provide insight into charge interaction inside the heterostructure. were determined using given Equation():

$\Delta\rho = \rho(GaTe/ MoS_2) - \rho(GaTe) - \rho(MoS_2)$,

where $\rho(GaTe/ MoS_2)$, $\rho(GaTe)$, and $\rho(MoS_2)$ are total charge density of the heterostructure, constituent single layers of GaTe and MoS2, respectively. The work function (Φ) is thermodynamic work (energy) for removing an electron from the surface to a point in the vacuum. It is not a characteristic of a bulk material rather a property of the surface of the material and was calculated using Equation ():

$\Phi = E_{vac} - E_F$, ()

where E_{vac} is the energy of a stationary electron in the vacuum at the surface, while E_F denotes the Fermi energy, which determines the electronic structure's ground state.

5.3. Results and Discussions

5.3.1 Schematic atomic structure of GaTe/MoS_2 with various Twist angle :

The schematic atomic structure of GaTe/ *MoS_2*heterostructure with various twist angles are shown in Fig. 5.1. The lattice mismatching varying between -0.77% to + 0.77% throughout all the twist angle. Simultaneously, the supercells at various rotation angles are geometrically optimised to acquire the associated lattice constants, which is to discover the optimal structure between finding the smallest lattice mismatch and the smallest number of supercell atoms.

Figure 5.1 Electronic Structure of GaTe/MoS_2 Heterostructure with various Twist angle of (a) 0°, (b) 10.89°, (c) 19.11°, (d) 40.89°, (e) 49.11°, (f) 60°

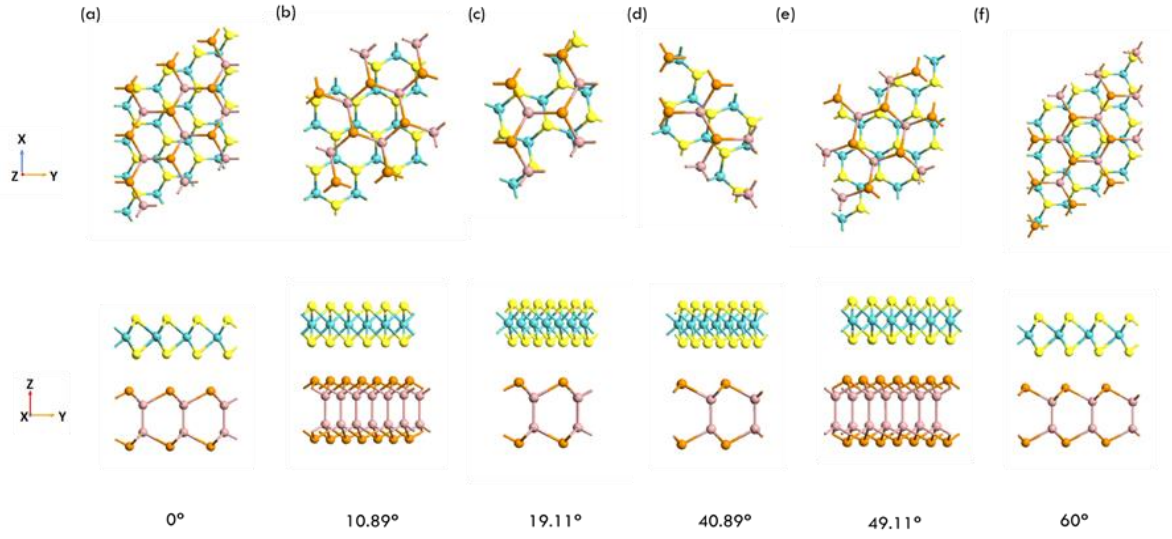

5.3.2 Projected Band structure at different interlayer twist

In Quantum-ATK, the Fat band structure are used to project contributions of different orbitals in the electronic band structure. We observed that with the varying twist angle, there is not much improvement in the band gap value, it is varying from 1.01 to 1.08 eV. However, the nature band structure remains indirect at all the twisted angles.***Figure 5.2*** *Fat band structure of*

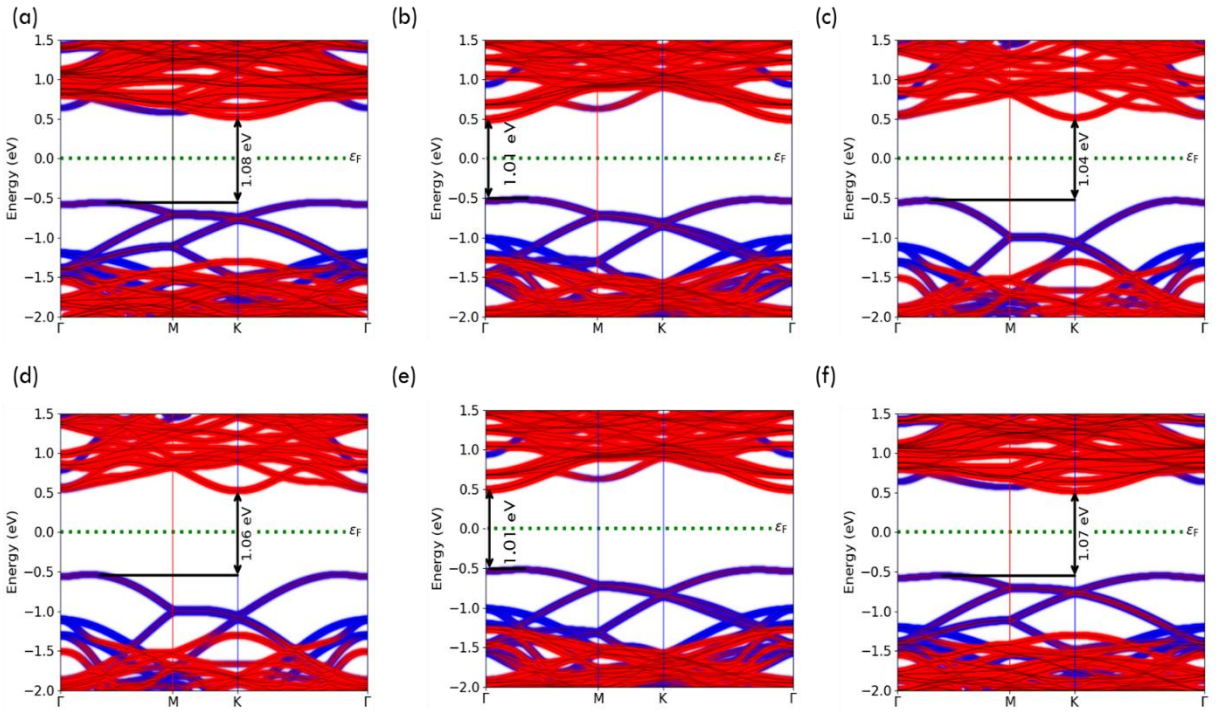

Figure 5.2 *GaTe/MoS_2 Heterostructure with various Twist angle of (a) 0°, (b) 10.89°, (c) 19.11°, (d) 40.89°, (e) 49.11°, (f) 60°*

In the figure red colour band is contributed by MoS_2 and the Blue colour band is contributed by GATe material. From the above figures it is clearly observable that the CBM is contributed by the MoS_2 monolayer On the other hand VBM is being contributed by GaTe monolayerSo the CBM and VBM is contributed by different materials. Here also one thing we can observe that the Fat Band structure is almost same for six different twist angles. The most important point is coming from these observations is that the Heterostructure GaTe/MoS_2 is essentially have a Type II band alignment. Another noticeable point in here is that the band gap is varying with different twist angle but the variation is very small (maximum 0.07 eV) . Along with this the heterostructure is a indirect band gap semiconductor at all six measured angles. For angle

0°, 19.11°, 40.89°, 60° the hetestructure is having transition from a from a point in between Γ and M to the point K and for 10.89°, 49.11° the heterostructure is having Γ to Γ transition.

5.3.3 Projected Density of States

The PDOS of GaTe/MoS_2 heterostructure at various interlayer twist angles are shown in Fig. 5.3. In the PDOS, we can visualize the more detail orbital contribution in the band structure. The figure clearly depicts that the CBM is coming from the 4d orbital of Mo atom and the VBM is coming from 5p orbital of Te atom. These results also support the previous Fat band structure estimation that the CBM and VBM are coming from different material

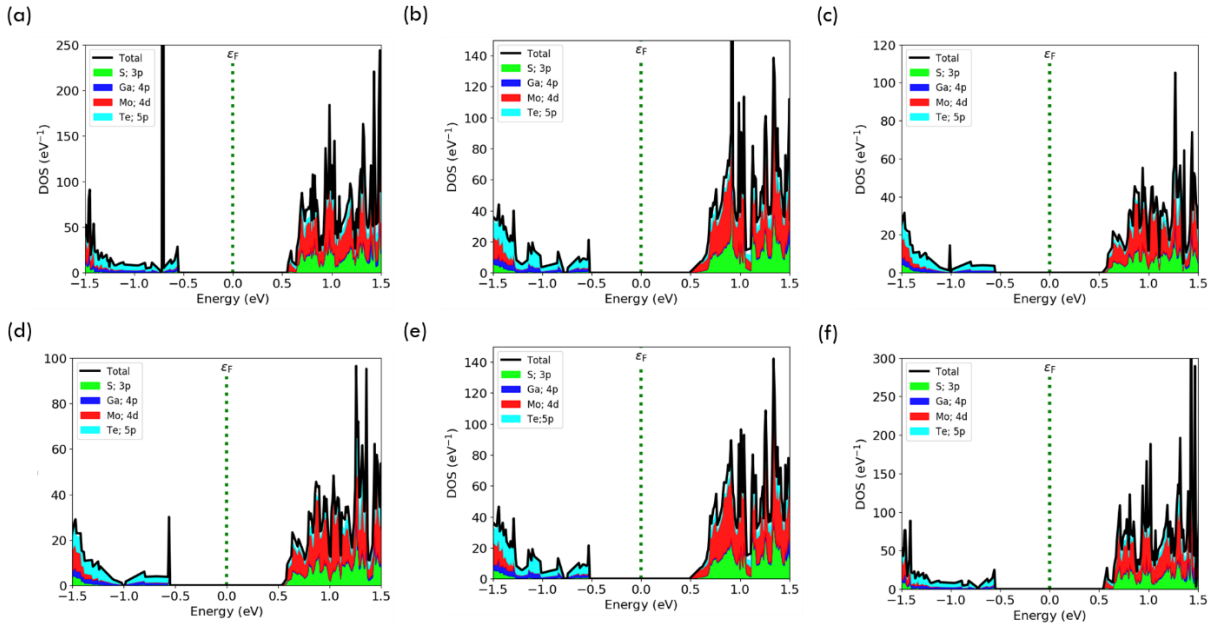

Figure 5.3 Projected Density of States of GATe/MoS_2 Heterostructure with various Twist angle of (a) 0°, (b) 10.89°, (c) 19.11°, (d) 40.89°, (e) 49.11°, (f) 60°

5.3.4 Optical Spectrum

The Optical spectrum is being evaluated for the optical analysis of GaTe/MoS_2 heterostructure. Here we have come up with very interesting observations. Firstly, for the 0°, 19.11°, 40.89°, 60° the heterostructure is having a good amount of optical absorption in the visible region. Secondly, for the 10.89°, 49.11° the heterostructure is having little amount of optical absorption in the visible region. The third thing which we can notice is that the optical spectrum of GaTe/MoS_2 heterostructure is actually three different pair of result that means for 0° and

60° the spectrum is overlapped and similarly for 10.89° and 49.11° and also for 19.11° and 40.89°. This is due to the concept of of mirror angle here. Simply mirror angles are pair of angles whose sum is 60° and the properties will be quite similar for the mirror angles. Here 0° and 60° , 10.89° and 49.11°, 19.11° and 40.89° are three set of mirror angles.

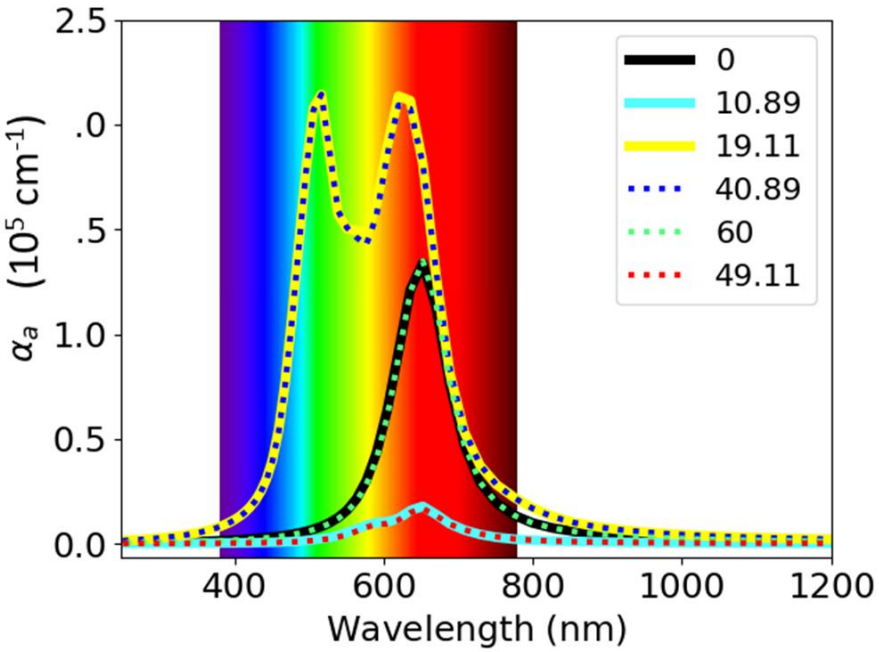

Figure 5.4 Optical Spectrum of GaTe/MoS_2 Heterostructure with various Twist angle of 0°, 10.89°, 19.11°, 40.89°, 49.11°, 60°

5.3.5 Effective potential (EP)l: The effective potentialV_{eff} [n] has three contributions [80]:

V_{eff} [n] =V_H [n] +V_{xc} [n] +V_{ext} [n]

The first two terms result from electron–electron interactions, that are affected by electron density. The first term, V^H [n], is the Hartree potential because of the mean-field electrostatic interaction among the electrons, while the second term, V^xc [n], is the exchange-correlation potential, which is a result of the electrons' quantum mechanical nature.

The EP plot for all twisted heterostructures is shown in Fig. 5.5. It is noted that there is not much change in the value of EP drop observed at the heterostructure.

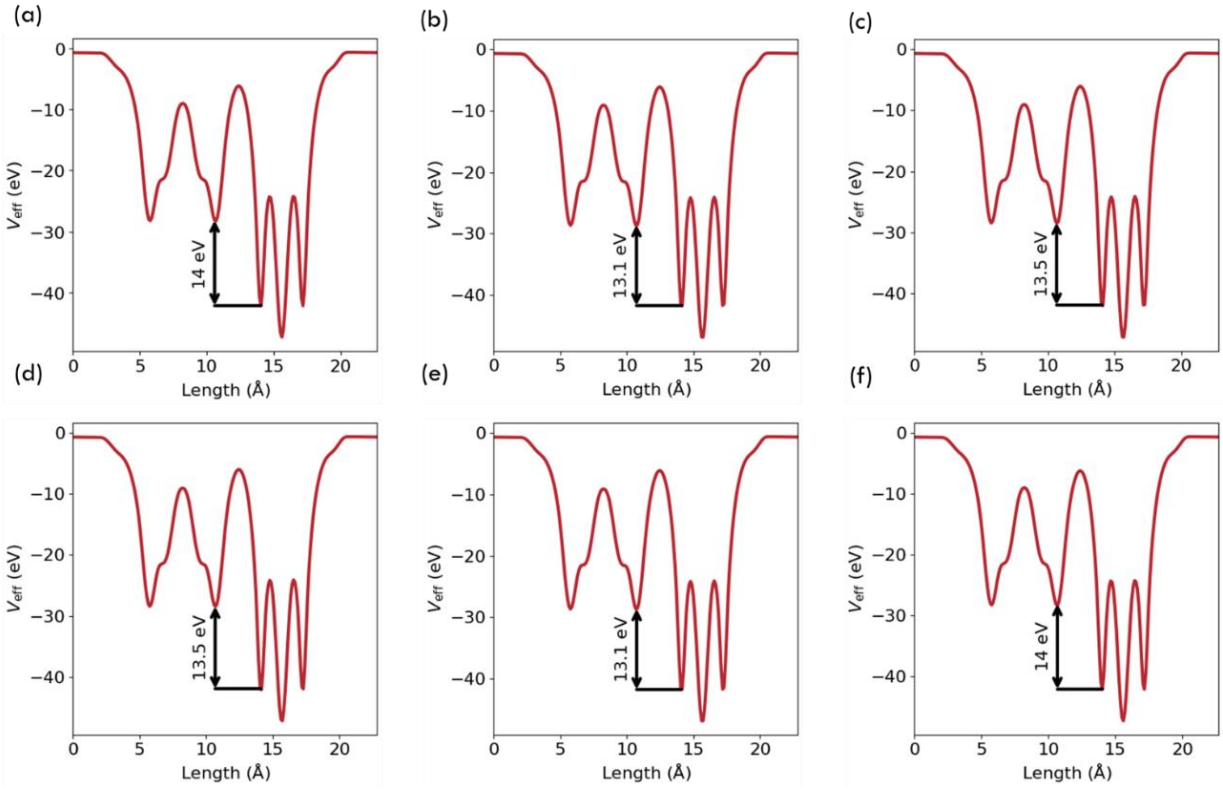

Figure 5.5 Effective Potential of GATe/MoS_2 Heterostructure with various Twist angle of (a) 0°, (b) 10.89°, (c) 19.11°, (d) 40.89°, (e) 49.11°, (f) 60°

Table.5.1 shows the all the calculated parameters for GaTe/MoS2 heterostructure are various interlayer twist angle.

Rotation Between Surfaces	Lattice Constant (a)	Interlayer Distance	Angle Between Surfaces	No. of atom	Strain (%)	Indirect Bandgap	Effective Potential(eV)
0°	12.58	3.26	120°	84	0.77	1.08	14
10.89°	10.95	3.30	60°	64	0.44	1.01	13.1
19.11°	8.34	3.32	120°	37	0.24	1.04	13.5
40.89°	8.34	3.36	60°	37	0.24	1.06	13.5
49.11°	10.95	3.30	120°	64	0.44	1.01	13.1
60°	12.58	3.23	120°	84	0.77	1.07	14

5.4 Conclusion

In conclusion, we used first-principles computations to examine the structural, electrical, and optical characteristics of GaTe/MoS_2 vdWH.. GaTe/MoS_2 vdWH is a type-II band aligned indirect band gap semiconductor in which charge transport from the MoS_2 layer to the GaTe layer Simultaneously, as compared to single layers, the GaTe/MoS_2 vdWH exhibits improved optical absorption capabilities in the visible light, near infrared, ranges. With using various interlayer twist angle, an excellent modulation in optical properties observed, although band structure remains type-II. The change in value of band gap at various twist angle is very small. These qualities, as well as the tunable electrical structure and optical properties of GaTe/ MoS_2 vdWH, open up new avenues for basic research and high-performance nanoelectronic applications and optoelectronic devices.

Chapter 6

Concluding Remark and Future Aspects

6.1 Research Implications

This thesis is revealing a wonderful study of Twistronics of 2D semiconductors. We have studied both homo bilayer of $MoSe_2$ and heterostructure of $GaTe/MoS_2$ heterostructures.. Our findings will be definitely helpful for future research on this domain. We found that the bilayer $MoSe_2$ can be converted to direct band gap semiconductor from an indirect band gap semiconductor at a certain magic angle. We also found that how the optical absorption of $GaTe/MoS_2$ structure is being modified at some angles can be used as a good candidate as photocatalyst.

6.2 Future Research Scope

Because of the large amount of rich science that has been revealed thus far, for a decades to come, moiré superlattice solids will undoubtedly be a vital source of intellectually intriguing scientific inventions.

Given the fact that the scientific community has access to hundreds of 2D materials, it is realistic to assume that once a larger number of scientists and engineers have access to high-quality 2D heterostructures that can be layered with predictable precision, a vast amount of quantum phenomenon will be discovered. Consider a bilayer heterostructure that can be built from hundred various 2D materials with, say, thirty different twisting angles (with one degree angular spacing). So, there would be 100×(30×100) = 300,000 different twisted two-dimensional materials, each with its own set of electrical, optical, magnetic, and other properties that potentially disclose new science. With a wider range of two-dimensional

materials, feasible twisting angles, and layer thicknesses, the real number might be significantly higher. When this study is extended to three levels, it yields 100× (30×100) × (30×100) = 9,00,000,000 tri-layer possibilities from hundred different two-dimensional materials. If there were a straightforward method for identifying and precisely creating the individuals that are most likely to be involved in these hypothesised one-in-a-million phenomena, even if one-in-a-million (or 900) of these combinations leads to non-trivial physical phenomena, this is enough to keep scientists and engineers engaged for the next decade, if not longer. To solve this seemingly insurmountable obstacle, multidisciplinary innovative and collaborative techniques are required.

References

1. Novoselov, K.S., et al., *Electric field effect in atomically thin carbon films.* science, 2004. **306**(5696): p. 666-669.

2. Cao, Y., et al., *Unconventional superconductivity in magic-angle Graphene superlattices.* Nature, 2018. **556**(7699): p. 43-50.

3. Cao, Y., et al., *Correlated insulator behaviour at half-filling in magic-angle Graphene superlattices.* Nature, 2018. **556**(7699): p. 80-84.

4. Yoo, H., et al., *Atomic and electronic reconstruction at the van der Waals interface in twisted bilayer Graphene.* Nature materials, 2019. **18**(5): p. 448-453.

5. Rickhaus, P., et al., *Transport through a network of topological channels in twisted bilayer Graphene.* Nano letters, 2018. **18**(11): p. 6725-6730.

6. Naik, M.H. and M. Jain, *Ultraflatbands and shear solitons in moiré patterns of twisted bilayer transition metal dichalcogenides.* Physical review letters, 2018. **121**(26): p. 266401.

7. Zhang, Y., et al., *Direct observation of a widely tunable band gap in bilayer Graphene.* Nature, 2009. **459**(7248): p. 820-823.

8. Mak, K.F., et al., *Observation of an electric-field-induced band gap in bilayer Graphene by infrared spectroscopy.* Physical review letters, 2009. **102**(25): p. 256405.

9. Ramasubramaniam, A., D. Naveh, and E. Towe, *Tunable band gaps in bilayer transition-metal dichalcogenides.* Physical Review B, 2011. **84**(20): p. 205325.

10. Jones, A.M., et al., *Spin–layer locking effects in optical orientation of exciton spin in bilayer WSe2.* Nature Physics, 2014. **10**(2): p. 130-134.

11. Fallahazad, B., et al., *Shubnikov–de Haas oscillations of high-mobility holes in monolayer and bilayer WSe 2: Landau level degeneracy, effective mass, and negative compressibility.* Physical review letters, 2016. **116**(8): p. 086601.

12. Lee, J.H., et al., *Reliable piezoelectricity in bilayer WSe2 for piezoelectric nanogenerators.* Advanced Materials, 2017. **29**(29): p. 1606667.

13. Xia, F., et al., *Two-dimensional material nanophotonics.* Nature Photonics, 2014. **8**(12): p. 899-907.

14. Katsnelson, M.I., *Graphene: carbon in two dimensions.* Materials today, 2007. **10**(1-2): p. 20-27.

15. Leng, X., et al., *Introduction to two-dimensional materials*, in *MOLECULAR INTERACTIONS ON TWO-DIMENSIONAL MATERIALS*. 2022, World Scientific. p. 1-41.

16. Roy, T., et al., *Field-effect transistors built from all two-dimensional material components.* ACS nano, 2014. **8**(6): p. 6259-6264.

17. Li, X. and Z. Sun, *Application of two-dimensional materials for electrochemical carbon dioxide reduction*, in *two-dimensional Nanomaterials for Energy Applications*. 2020, Elsevier. p. 289-326.

18. Naumis, G.G., *Electronic properties of two-dimensional materials*, in *Synthesis, Modeling, and Characterization of two-dimensional Materials, and Their Heterostructures*. 2020, Elsevier. p. 77-109.

19. Somvanshi, D. and S. Jit, *Transition metal dichalcogenides based two-dimensional heterostructures for optoelectronic applications*, in *two-dimensional Nanoscale Heterostructured Materials*. 2020, Elsevier. p. 125-149.

20. Baseden, K.A. and J.W. Tye, *Introduction to density functional theory: calculations by hand on the helium atom.* Journal of Chemical Education, 2014. **91**(12): p. 2116-2123.

21. Dharmawardana, M., *A Review of Studies on Strongly-Coupled Coulomb Systems Since the Rise of DFT and SCCS-1977.* Contributions to Plasma Physics, 2015. **55**(2-3): p. 85-101.

22. Blaha, P., et al., *WIEN2k: An APW+ lo program for calculating the properties of solids.* The Journal of Chemical Physics, 2020. **152**(7): p. 074101.

23. Rindt, C. and S. Gaastra-Nedea, *Modeling thermochemical reactions in thermal energy storage systems*, in *Advances in Thermal Energy Storage Systems*. 2015, Elsevier. p. 375-415.

24. Sahni, V., *Quantal density functional theory*, in *Quantal Density Functional Theory*. 2016, Springer. p. 67-133.

25. Kurth, S., M.A.L. Marques, and E.K.U. Gross, *Density-Functional Theory*, in *Encyclopedia of Condensed Matter Physics*, F. Bassani, G.L. Liedl, and P. Wyder, Editors. 2005, Elsevier: Oxford. p. 395-402.

26. Ausín, V. and J.A. Rivas, *Gamma-ray-induced color in Ca F 2 at room temperature: Coloring kinetics and thermal annealing.* Physical Review B, 1974. **9**(2): p. 775.

27. Hennighausen, Z. and S. Kar, *Twistronics: A turning point in two-dimensional quantum materials.* Electronic Structure, 2021. **3**(1): p. 014004.

28. Wu, D., Y. Pan, and T. Min, *Twistronics in Graphene, from transfer assembly to epitaxy.* Applied Sciences, 2020. **10**(14): p. 4690.

29. Zeller, P., X. Ma, and S. Günther, *Indexing moiré patterns of metal-supported Graphene and related systems: strategies and pitfalls.* New Journal of Physics, 2017. **19**(1): p. 013015.

30. Zeller, P. and S. Günther, *What are the possible moiré patterns of Graphene on hexagonally packed surfaces? Universal solution for hexagonal coincidence lattices, derived by a geometric construction.* New Journal of Physics, 2014. **16**(8): p. 083028.

31. Rost, F., et al., *Nonperturbative theory of effective hamiltonians for deformations in two-dimensional materials: Moiré systems and dislocations.* Physical Review B, 2019. **100**(3): p. 035101.

32. Lebanon, G. and A.M. Bruckstein, *Variational approach to moiré pattern synthesis.* JOSA A, 2001. **18**(6): p. 1371-1382.

33. Lebanon, G. and A.M. Bruckstein, *On Designing Moiré Patterns*, in *Visual Attention Mechanisms*. 2002, Springer. p. 205-217.

34. Kim, J.H., K. Kim, and Z. Lee, *The hide-and-seek of grain boundaries from moiré pattern fringe of two-dimensional Graphene.* Scientific reports, 2015. **5**(1): p. 1-9.

35. Hennighausen, Z., et al., *Evidence of a purely electronic two-dimensional lattice at the interface of TMD/Bi 2 Se 3 heterostructures.* Nanoscale, 2019. **11**(34): p. 15929-15938.

36. Lu, X., et al., *Superconductors, orbital magnets and correlated states in magic-angle bilayer Graphene.* Nature, 2019. **574**(7780): p. 653-657.

37. Yankowitz, M., et al., *Tuning superconductivity in twisted bilayer Graphene.* Science, 2019. **363**(6431): p. 1059-1064.

38. Cao, Y., et al., *Magic-angle Graphene superlattices: a new platform for unconventional superconductivity.* arXiv preprint arXiv:1803.02342, 2018.

39. Sharpe, A.L., et al., *Emergent ferromagnetism near three-quarters filling in twisted bilayer Graphene.* Science, 2019. **365**(6453): p. 605-608.

40. Shallcross, S., S. Sharma, and O.A. Pankratov, *Quantum interference at the twist boundary in Graphene.* Physical review letters, 2008. **101**(5): p. 056803.

41. Castro, E.V., et al., *Biased bilayer Graphene: semiconductor with a gap tunable by the electric field effect.* Physical review letters, 2007. **99**(21): p. 216802.

42. McCann, E., D.S. Abergel, and V.I. Fal'ko, *Electrons in bilayer Graphene.* Solid state communications, 2007. **143**(1-2): p. 110-115.

43. Dos Santos, J.L., N. Peres, and A.C. Neto, *Graphene bilayer with a twist: electronic structure.* Physical review letters, 2007. **99**(25): p. 256802.

44. Varchon, F., et al., *Rotational disorder in few-layer Graphene films on 6 H− Si C (000− 1): A scanning tunneling microscopy study.* Physical Review B, 2008. **77**(16): p. 165415.

45. Latil, S., V. Meunier, and L. Henrard, *Massless fermions in multilayer graphitic systems with misoriented layers: Ab initio calculations and experimental fingerprints.* Physical Review B, 2007. **76**(20): p. 201402.

46. Hass, J., et al., *Why multilayer Graphene on 4 H− SiC (000 1) behaves like a single sheet of Graphene.* Physical review letters, 2008. **100**(12): p. 125504.

47. Huang, J.Y., et al., *In situ observation of Graphene sublimation and multi-layer edge reconstructions.* Proceedings of the National Academy of Sciences, 2009. **106**(25): p. 10103-10108.

48. Das, S., et al., *Beyond Graphene: progress in novel two-dimensional materials and van der Waals solids.* Annual Review of Materials Research, 2015: p. 1-27.

49. Zhang, Z., et al., *Interface Engineering of Band Evolution and Transport Properties of Bilayer WSe2 with Different Electric Fields.* The Journal of Physical Chemistry C, 2019. **123**(32): p. 19812-19819.

50. Joseph, I., et al., *Interlayer angle-dependent electronic structure and optoelectronic properties of BP-MoS2 heterostructure: a first principle study.* Computational Materials Science, 2021. **186**: p. 110056.

51. Zhao, X., L. Li, and M. Zhao, *Lattice match and lattice mismatch models of Graphene on hexagonal boron nitride from first principles.* Journal of Physics: Condensed Matter, 2014. **26**(9): p. 095002.

52. Mele, E.J., *Commensuration and interlayer coherence in twisted bilayer Graphene.* Physical Review B, 2010. **81**(16): p. 161405.

53. Shallcross, S., S. Sharma, and O.A. Pankratov, *Twist boundary in Graphene: energetics and electric field effect.* Journal of Physics: Condensed Matter, 2008. **20**(45): p. 454224.

54. Geng, W., et al., *Angle Dependence of Interlayer Coupling in Twisted Transition Metal Dichalcogenide Heterobilayers.* The Journal of Physical Chemistry C, 2020. **125**(1): p. 1048-1053.

55. Yao, X. and X. Zhang, *Electronic Structures of Twisted Bilayer InSe/InSe and Heterobilayer Graphene/InSe.* ACS omega, 2021. **6**(20): p. 13426-13432.

56. Zhu, Y., et al., *The twist angle has weak influence on charge separation and strong influence on recombination in the MoS 2/WS 2 bilayer: ab initio quantum dynamics.* Journal of Materials Chemistry A, 2022. **10**(15): p. 8324-8333.

57. Wang, Q.H., et al., *Electronics and optoelectronics of two-dimensional transition metal dichalcogenides.* Nature nanotechnology, 2012. **7**(11): p. 699-712.

58. Kállay, M. and P.R. Surján, *Higher excitations in coupled-cluster theory.* The Journal of chemical physics, 2001. **115**(7): p. 2945-2954.

59. Boys, S.F. and F. Bernardi, *The calculation of small molecular interactions by the differences of separate total energies. Some procedures with reduced errors.* Molecular Physics, 1970. **19**(4): p. 553-566.

60. Grimme, S., *Semiempirical GGA-type density functional constructed with a long-range dispersion correction.* Journal of computational chemistry, 2006. **27**(15): p. 1787-1799.

61. Grimme, S., *Accurate description of van der Waals complexes by density functional theory including empirical corrections.* Journal of computational chemistry, 2004. **25**(12): p. 1463-1473.

62. Liu, D.C. and J. Nocedal, *On the limited memory BFGS method for large scale optimization.* Mathematical programming, 1989. **45**(1): p. 503-528.

63. Ye, M., et al. *Recent advancement on the optical properties of two-dimensional molybdenum disulfide (MoS2) thin films*. in *Photonics*. 2015. Multidisciplinary Digital Publishing Institute.

64. Becke, A.D. and K.E. Edgecombe, *A simple measure of electron localization in atomic and molecular systems.* The Journal of chemical physics, 1990. **92**(9): p. 5397-5403.

65. Meckbach, L., T. Stroucken, and S.W. Koch, *Giant excitation induced band gap renormalization in TMDC single layers.* Applied Physics Letters, 2018. **112**(6): p. 061104.

66. Meckbach, L., T. Stroucken, and S.W. Koch, *Influence of the effective layer thickness on the ground-state and excitonic properties of transition-metal dichalcogenide systems.* Physical Review B, 2018. **97**(3): p. 035425.

67. Guo, Y., et al., *Oxidation resistance of monolayer group-IV monochalcogenides.* ACS Applied Materials & Interfaces, 2017. **9**(13): p. 12013-12020.

68. Do, D.T., S.D. Mahanti, and C.W. Lai, *Spin splitting in two-dimensional monochalcogenide semiconductors.* Scientific Reports, 2015. **5**(1): p. 1-9.

69. Schumann, H. and L. Gmelin, *Gmelin handbook of inorganic and organometallic chemistry: Sn. Organotin compounds. Tin centered radicals, tin (II) compounds, compounds with tin element double bonds tin (II) complexes with aromatic systems, stannacarboranes, and other organotin compounds/authors Herbert Schumann; Ingeborg Schumann. Formula index Rainer Bohrer... Ed. Ulrich Krüerke..... Pt. 23*. 1995: Springer.

70. Mak, K.F., et al., *Atomically thin MoS 2: a new direct-gap semiconductor.* Physical review letters, 2010. **105**(13): p. 136805.

71. Lin, M.-W., et al., *Mobility enhancement and highly efficient gating of monolayer MoS2 transistors with polymer electrolyte.* Journal of Physics D: Applied Physics, 2012. **45**(34): p. 345102.

72. Song, J.C. and N.M. Gabor, *Electron quantum metamaterials in van der Waals heterostructures.* Nature nanotechnology, 2018. **13**(11): p. 986-993.

73. Robinson, J.A., *Growing vertical in the flatland.* ACS nano, 2016. **10**(1): p. 42-45.

74. Jakubczyk, T., et al., *Radiatively limited dephasing and exciton dynamics in MoSe2 single layers revealed with four-wave mixing microscopy.* Nano letters, 2016. **16**(9): p. 5333-5339.

75. Ponomarenko, L., et al., *Cloning of Dirac fermions in Graphene superlattices.* Nature, 2013. **497**(7451): p. 594-597.

76. Dean, C.R., et al., *Hofstadter's butterfly and the fractal quantum Hall effect in moiré superlattices.* Nature, 2013. **497**(7451): p. 598-602.

77. Lane, C., *Interlayer coupling induced quasiparticles.* Physical Review B, 2020. **101**(23): p. 235138.

78. Zribi, B., et al., *A microfluidic electrochemical biosensor based on multiwall carbon nanotube/ferrocene for genomic DNA detection of Mycobacterium tuberculosis in clinical isolates.* Biomicrofluidics, 2016. **10**(1): p. 014115.

79. Chen, S., et al., *Adsorption/desorption and electrically controlled flipping of ammonia molecules on Graphene.* New Journal of Physics, 2010. **12**(12): p. 125011.

80. Cococcioni, M. and S. De Gironcoli, *Linear response approach to the calculation of the effective interaction parameters in the LDA+ U method.* Physical Review B, 2005. **71**(3): p. 035105.

81. Zhou, J., et al., *two-dimensionalMatPedia, an open computational database of two-dimensional materials from top-down and bottom-up approaches.* Scientific data, 2019. **6**(1): p. 1-10.

82. Rasmussen, F.A. and K.S. Thygesen, *Computational two-dimensional materials database: electronic structure of transition-metal dichalcogenides and oxides.* The Journal of Physical Chemistry C, 2015. **119**(23): p. 13169-13183.

83. Pan, J. and Q. Yan, *Data-driven material discovery for photocatalysis: a short review.* Journal of Semiconductors, 2018. **39**(7): p. 071001.

84. Choudhary, K., K.F. Garrity, and F. Tavazza, *High-throughput discovery of topologically non-trivial materials using spin-orbit spillage.* Scientific reports, 2019. **9**(1): p. 1-8.

85. Choudhary, K., et al., *Accelerated discovery of efficient solar cell materials using quantum and machine-learning methods.* Chemistry of Materials, 2019. **31**(15): p. 5900-5908.

86. Masubuchi, S., et al., *Autonomous robotic searching and assembly of two-dimensional crystals to build van der Waals superlattices.* Nature communications, 2018. **9**(1): p. 1-12.